# Review of High-Temperature Power Electronics Converters

Yudi Xiao, *Member, IEEE*, Zhe Zhang, *Senior Member, IEEE*, Martijn Sebastiaan Duraij, *Student Member, IEEE*, Tiberiu-Gabriel Zsurzsan, *Member, IEEE*, and Michael A. E. Andersen, *Member, IEEE*

***Abstract*—Power electronics converters operating at elevated temperature usually have degraded performance, such as reduced efficiency, lower noise immunity, and decreased system reliability, compared to those operating at room temperature. Nevertheless, harsh-environment applications, such as deep earth drilling, automotive, avionics, and space exploration, have been utilizing converters in high-temperature environments and are continuously pushing the temperature limits higher and higher with the advances in device technologies and converter design methodologies. This article starts with a literature study to identify the temperature dependence and the temperature limits of individual components. Then, published works about high-temperature converters are examined. Their selection of components is compared. Experimental results are analyzed to reflect on the efficacy of different component selections. Finally, since the latest published high-temperature converter was developed more than five years ago, a 1-kV input, 520-V output, 1-kW, 150 °C-ambient-temperature-rated dc–dc converter is designed with state-of-the-art devices. Based on the literature review, and the test of the 150 °C prototype, the main challenges of designing high-temperature power electronics converters are identified and concluded to be time-consuming, difficult, and expensive characterization of components, lack of accurate and computationally efficient models of converters, and optimizing component selection within short development time.**

***Index Terms*—Design automation, high-temperature power electronics, temperature drift.**

## I. Introduction

POWER electronics converters have found their way into many applications, e.g., switched-mode power supplies in adapters and chargers, motor drives, and solid-state transformers to interconnect electric grids. Some applications have been calling for power electronics converters that can operate in high-temperature environment [1], [2]. For example, in oil and gas applications, the downhole electronics usually operate at 150–175 °C ambient temperature. Due to the declining reserve of easily accessible natural resources, the industry tends to drill deeper. The operating temperature in these hostile wells may exceed 200 °C. In automotive and avionics applications, in order to reduce the cost, weight, and volume of wiring, sensors and electric circuits are being moved closer and closer to engines, brakes, etc., where temperature exceeds 125 °C [3]. The trend to replace purely mechanical and hydraulic systems in vehicles and aircraft with electromechanical or mechatronic systems demands high-temperature power electronics as well, because these power electronics converters need to be close to the actuators [4]. Space exploration is one of the most exciting applications where high-temperature power electronics play critical roles [5]. The NASA Mars Curiosity Rover, as an example, used motor drivers that were specified at up to 125 °C ambient temperature [6].

Traditionally, there are two ways to ensure safe operation of power electronics converters in a high-temperature environment. One is using coolant to keep converters cool, and the other is utilizing protective enclosures to prevent the environment from heating up converters. The main drawback of these two solutions is that the installation of cooling or enclosure system increases the cost, volume, and weight of the converters. Moreover, it is not practical to use either coolant or protective enclosures in deep-earth applications [1]. Therefore, ideally, industries would prefer reliable power electronics that can withstand high temperature by itself. As concluded in [7], and further emphasized in [2], operating electronics at high temperature is a system problem. A power electronics converter is a system hosting power semiconductor devices, inductors, transformers, capacitors, resistors, gate drive circuits, measurement circuits, microcontrollers, printed circuit board (PCB), and solders. Failure or function degradation from any part of a power electronics converter may cause the entire converter to malfunction. The uncertainty of the performance and the lifetime of individual components at high temperature make it challenging to design and operate converters properly, in particular, in a wide temperature range. Therefore, high-temperature converter design is indeed a critical and emerging topic as it will fertilize our knowledge about power electronics on both component level and system level, especially when wide band-gap devices are deployed. However, due to the limited market size of high-temperature converters

Manuscript received 22 August 2021; revised 22 November 2021; accepted 15 January 2022. Date of publication 4 February 2022; date of current version 6 September 2022. This work was supported by Innovation Fund Denmark (IFD) under Grant 8053-00095B. Recommended for publication by Associate Editor K. Wada. *(Corresponding author: Zhe Zhang.)*

Yudi Xiao, Martijn Sebastiaan Duraij, Tiberiu-Gabriel Zsurzsan, and Michael A. E. Andersen are with the Department of Electrical Engineering, Technical University of Denmark, DK-2800 Kongens Lyngby, Denmark (e-mail: yudixiaojd@outlook.com; msdu@elektro.dtu.dk; tgzsur@elektro.dtu.dk; ma@elektro.dtu.dk).

Zhe Zhang is with the Hebei University of Technology, Tianjin 300401, P.R.China, and also with the Technical University of Denmark, DK-2800 Kgs. Lyngby, Denmark (e-mail: zhezhangdtu@outlook.com).

Color versions of one or more figures in this article are available at https://doi.org/10.1109/TPEL.2022.3148192.

Digital Object Identifier 10.1109/TPEL.2022.3148192

and the preference of designers to keep their design confidential, the number of related publications is relatively small. There is no standard about the qualification of components and converters operating at ambient temperature more than 150 °C. Moreover, there is no publication dedicated on giving an overview of high-temperature power electronics converters. Thus, this article presents a review of high-temperature converters. This review article starts with studying components' high-temperature performance, followed by a comparison of published designs of converters for high-temperature applications, and finally ends with a case study of designing a 150 °C rated converter with state-of-the-art components. Lifetime of components and converters stressed under high temperature is not discussed in this article, because, as mentioned, there is not any international standards regulating the procedure of qualification yet.

The rest of this article is organized as follows. Section II presents the performance of electronic components stressed under high temperature. The highest operating temperature of state-of-the-art electronic components is identified. Considering the temperature limits of components, the maximum ambient temperature of the state-of-the-art power electronics converters is estimated to be in the range of 210–240 °C. In Section III, power electronics converters with maximum temperature rating between 150 and 240 °C are reviewed. 150 °C is selected as the low end of the temperature scale, because normally 150 °C is the maximum temperature rating specified in the datasheets of standard-temperature components. The converter review shows that designing high-temperature converters would be very expensive if high-temperature components (rated $> 200$ °C) are used. Actually, most of the published high-temperature converters use standard-temperature components well above their specifications to reduce cost. Therefore, characterizing standard-temperature components over temperature is needed. In addition to component characterization, component selection is another challenging task, because a trade-off between the quality of design output and development time has to be made properly. In Section IV, in the light of that the latest published high-temperature converter was developed and reported five years ago, a 1-kV input, 520-V output, 1-kW dc–dc converter is designed as a case study with state-of-the-art standard-temperature components. The design flow is an automated procedure. The prototype is tested in a 150 °C environment. Finally, Section V concludes this article.

## II. Components Operating At High Temperature

### A. Power Semiconductor Devices—Die Material

The physical effects that degrade the performance of semiconductor dies at high temperature have been well summarized in [7]. The increasing intrinsic carrier density and junction leakage current with temperature are the two primary physical effects that limit the functionality of p–n junctions at high temperature. The intrinsic carrier density $n_i$ of a semiconductor can be expressed by [8]

$$n_i = 2\left(\frac{2\pi kT}{h^2}\right)^{3/2}(m_{dh}m_{de})^{3/4} e^{-E_g/2kT} \quad (1)$$

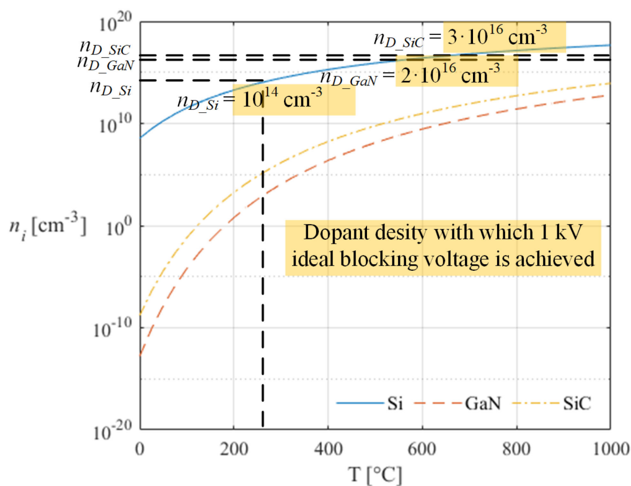


Fig. 1. $n_i$ versus $T$ of Si, SiC, and GaN at bandgap energy 1.12, 3, and 3.39 eV, respectively.

where $k$ and $h$ are Boltzmann's and Planck's constants. $T$ is the temperature. $m_{dh}$ and $m_{de}$ are the hole and electron effective masses. $E_g$ is the bandgap energy. As shown, $n_i$ depends on temperature and the bandgap of a semiconductor. Small bandgap and high temperature may increase intrinsic carrier density. To prevent the semiconductor junction from being "washed out," the intrinsic carrier density needs to be smaller than the dopant density $n_D$, which is limited by the breakdown voltage of p–n junctions [7]. Based on (1), the intrinsic carrier density of silicon (Si), silicon carbide (SiC), and gallium nitride (GaN) at different temperatures can be calculated, and is shown in Fig. 1. As expected, SiC and GaN have much smaller $n_i$ than Si due to their large bandgap energy. Fig. 1 also illustrates the limitation of $n_i$ set by $n_D$. To have a 1-kV ideal blocking voltage, the dopant density of Si $n_{D_Si}$ needs to be smaller than $10^{14}$ cm$^{-3}$ [9]. Therefore, ideally, to ensure the functionality of Si with a capability of blocking 1 kV, the temperature of Si has to be lower than 250 °C. In contrast, with the same 1-kV ideal blocking voltage, the intrinsic carrier density of SiC and GaN will not exceed the dopant density even though the temperature is up to 1000 °C. The large bandgap energy of SiC and GaN also results in low junction leakage current, which changes exponentially with respect to $\frac{kT}{E_g}$.

Moreover, many applications demand for power electronics converters capable of operating not only at high temperature but also over a wide temperature range. Therefore, we need to consider device parameter variations, e.g., threshold voltage and on resistance of MOSFETs, over temperature. On the die level, the primary physical effects that decide these parameter variations are the decreasing bandgap energy, carrier mobility $\mu_e$ and $\mu_h$ (e, electron; h, hole), saturation velocity $v_{sat}$, thermal conductivity $K$, and the changing breakdown electric field $E_{BR}$ of semiconductors with temperature [11]. Since the dependency of some of these physical properties on temperature varies with doping level, it is hard to conclude which semiconductor material has the least temperature dependency [12]. Table I gives the typical $E_g$, $\mu_e$, $\mu_h$, $v_{sat}$, $K$, and $E_{BR}$ of Si, SiC, and GaN at 25 and 200 °C, respectively. Both SiC and GaN show noticeable dependency

TABLE I
ELECTRICAL PROPERTIES OF SI, SIC, AND GAN AT 25 AND 200 °C

| | Si @ 25 °C | Si @ 200 °C | SiC @ 25 °C | SiC @ 200 °C | GaN @ 25 °C | GaN @ 200 °C |
|---|---|---|---|---|---|---|
| $E_g$ [eV] | 1.17 [13] | 1.07 [13] | 2.86 [14] | 2.79 [14] | 3.18 [15] | 3.11 [15] |
| $\mu_e$ [cm$^2$V$^{-1}$s$^{-1}$] @ $n_D \approx 2\times10^{17}$cm s$^{-3}$ | 900 [16] | 300 [16] | 200 [17] | 100 [17] | 2000 [18] | not found |
| $\mu_h$ [cm$^2$V$^{-1}$s$^{-1}$] @ $n_D \approx 2\times10^{17}$cm s$^{-3}$ | 200 [16] | <100 [16] | not found | not found | not found | not found |
| $v_{sat}$ [$\times10^7$cm s$^{-1}$] | 0.85 [19] | not found | 2 [11] | 1.55 [11] | 2.2 [11] | 2.02 [11] |
| $K$ [W m$^{-1}$K$^{-1}$] non-doped | 200 [20] | 90 [20] | 500 [11] [21] | 230 [11] | 125 [11] | 100 [11] |
| $E_{BR}$ [kV cm$^{-1}$] | ≈300 | >300 | ≈2400 | <2400 | ≈5000 | >5000 |

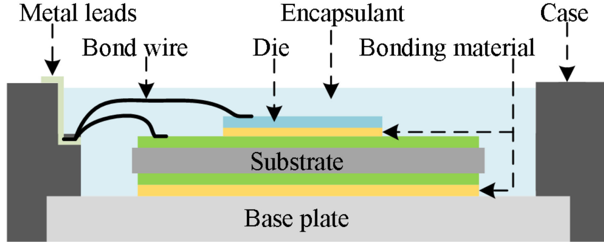


Fig. 2. Conceptual drawing of a packaged power semiconductor device [25].

on temperature in terms of the listed physical properties. At 200 °C, GaN seems to still hold the highest carrier mobility and saturation velocity, which make GaN the better choice for high-current and high-frequency operations. The superiority of SiC to GaN is due to SiC's high thermal conductivity, which makes SiC devices better toward high power density and high reliability. The breakdown electric field of GaN is more than twice that of SiC's. However, due to the challenging GaN crystal growth process, most of the commercial GaN power devices are built on foreign substrates, among which Si is still the most common option due to its low cost [24]. The breakdown voltage of these GaN-on-Si devices is limited by the Si substrate [24]. The maximum breakdown voltage of commercial GaN transistors is 900 V.

### *B. Power Semiconductor Devices-Packaging*

Semiconductor technologies rapidly advance forward, and have promising properties at high temperature. For example, Table I presents that SiC and GaN at 200 °C still outperform Si at 25 °C. However, low-cost commercial power semiconductor devices for > 175 °C operation are still difficult to find. Given that, packaging is the major limiting factor. A packaged power semiconductor device consists of power semiconductor die, bonding material for die and substrate attach, substrate, base plate, bond wires, encapsulant, and case, as shown in Fig. 2 [25].

In large high-power die attach for 200–300 °C operation, the majority of binding materials are lead-based systems, such as lead-tin (Pb-Sn), due to their high ductility, acceptable thermal conductivity and cost, and well-established knowledge base of physical properties and manufacturing process of leaded solders [26]. However, lead poses great threat to human health and environment. The most popular lead-free die attach method for up to 300 °C operation is low-temperature silver (Ag) sintering, thanks to the high electrical and thermal conductivity of bluk Ag, and the low-temperature and low(no)-pressure sintering process [27]. Currently, there is few effective methods in large high-power die attach for over 300 °C operations.

Direct-bonded copper (DBC), which has been widely used as substrates in < 175 °C rated packages, can be used for 175–250 °C operations as well. The ceramic layer sandwiched between the copper layers can withstand high temperature. The primary challenge is to minimize the thermomechanical stress due to the mismatch of coefficient of thermal expansion (CTE) of die, bonding material, and substrate [28]. Additionally, the substrate should have high thermal conductivity and high electrical resistivity. Aluminium nitride (AlN) and aluminium oxide ($Al_2O_3$) are the commonly used ceramic for substrates. Compared to $Al_2O_3$, AlN has higher thermal conductivity, and closer CTE to SiC and GaN, but higher cost. To have high reliability at elevated temperature, AlN is usually preferred as the ceramic material in substrate [29], [30]. Other than DBC, direct-bonded aluminum (DBA) can also be used to make substrates [31]. Due to surface roughening of aluminum in large-temperature cycling (for example, −55 to 250 °C in [32]), DBA is rarely used in high-temperature power semiconductor packages.

Bond wire break or lift is another failure mode of power semiconductor packages [25]. To have reliable wire bonding at high temperature or over a wide temperature range, the material of bond wire and the metalization of bonding pad need to be carefully selected [33]. Preferably, the same material should be used for bond wire and metalization of bonding pad, since interdiffusion and interface corrosion occur between dissimilar metals at high temperatures, which degrade bond strength. Commercial bare die SiC MOSFETs and diodes, such as those from CREE, use Al as top-side pads metalization. Because of that, laboratory power semiconductor/module packages for 175–250 °C operation have been using Al bond wires [34], [35]. Since Al and Nickel (Ni) bond has been proved to be reliable at up to 350 °C, the copper layers on substrate are usually Ni-plated [36]. Other than Al and Ni bonds, gold (Au) wire bonded to a gold pad is extremely reliable. However, the high cost of gold makes it not favorable in large high-power die packaging, which requires more raw material than small low-power dies.

As a substrate holds dies, a base plate is needed to hold the entire packaged device, and to dissipate heat to heat sinks. Therefore, it is necessary for a base plate to have certain mechanical strength, high thermal conductivity, and matched CTE with substrate's. A summary of commonly used materials for base plates has been given in [34]. Base plates made of pure copper (Cu) are usually not used in high temperature due to Cu's CTE mismatches with AlN's. Metal matrix composites (MMC) are often utilized since their CTE can be tailored to match with that of the substrates.

The case protects a package from vibrations, mechanical shocks, and environmental effects. Cases of < 175 °C rated

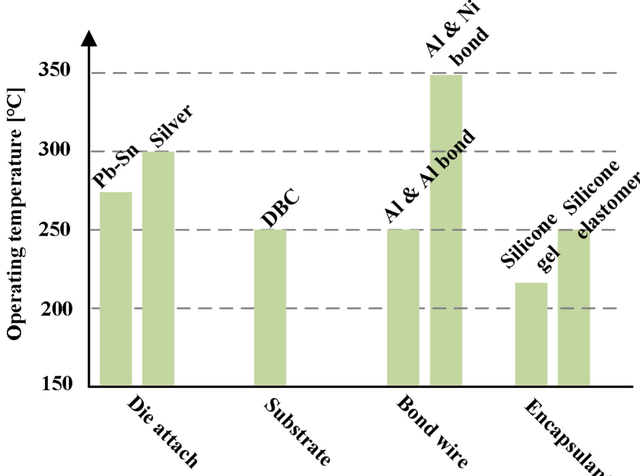


Fig. 3. Summary of temperature limits from power semiconductor packaging.

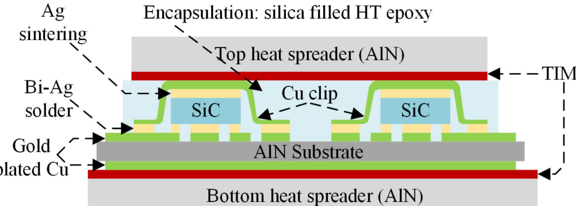


Fig. 4. Conceptual drawing of the 220 °C-rated SiC DMOSFET flip-chip power module (1200 V, 160 mΩ per chip) presented in [51] and [52]. TIM, thermal interface material.

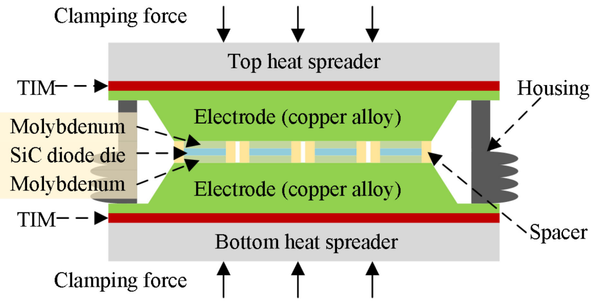


Fig. 5. Conceptual drawing of the 150 °C-rated 3.1-kV 600-A SiC diode press-pack module presented in [53].

packages are usually made of plastics such as thermoset allyls (DAP) and thermoset epoxy [25]. The glass transition temperature $T_g$ of these plastics is around 160 °C. For $>$ 175 °C operation, ceramic or metal cases can be used [37]–[40].

The main function of encapsulant is to protect dies and bonding wires from environmental effects, e.g., moisture diffusion, chemical contamination [41]. Preferably, the encapsulant should also increase dielectric strength and heat dissipation inside of the package. Hence, the voltage rating and thermal conductance of the package get increased [25]. Therefore, long-term stability of encapsulant's properties is a key factor to address, in order to make a reliable package. Polymers have been widely used as encapsulant in $<$ 175 °C rated packages, and can be divided into two categories: 1) soft encapsulants such as silicone gel, whose $T_g$ is lower than the lowest operating temperature, and 2) hard encapsulants such as silicone elastomer, whose $T_g$ is higher than the highest operating temperature. The operation limits of silicone gels are 250 °C and 100 h or 220 °C and 400 h, above which the gels either crack or have complete degradation [42]. Silicone elastomers are more reliable than silicone gels. They do not show cracks at 250 °C and 500 h thermal storage test [42]. However, the dielectric strength of silicone elastomers drastically decreases with temperature. In [43], the three silicone elastomer samples show 30%–40% decrease of dielectric strength when temperature increases from 20 to 250 °C. Therefore, reliable $>$ 175 °C rated packages call for new encapsulation materials [44].

The above discussion about the temperature limits of different parts of a power semiconductor package is summarized in Fig. 3. As shown, currently, the maximum temperature rating of packaged power semiconductor devices is likely to be around 220 °**C**, and is limited by the encapsulant material.

Apart from packaging material, packaging scheme is also a prominent factor that affects a power semiconductor package's electrical and thermal performance at high temperature. The drawing in Fig. 2 is an example of wire-bonding packaging scheme, which is widely used in manufacturing room-temperature power semiconductor devices. Manufacturers prefer sticking to wire-bonding packaging scheme for high-temperature products. With this scheme, standard equipment and procedures can be used, and hence, the cost of manufacturing new products can be kept low. Table II gives a summary of the published high-temperature power semiconductor modules using wire-bonding. With proper selection of materials and assembly methods, wire-bonding packages can operate at high ambient temperature (200–250 °C). However, [45]–[48] do not show any measurements on life time of wire-bonding packages at high ambient temperature.

Although cost-effective, wire-bonding packaging scheme has three major limitations. First, it only allows heat to dissipate through the base plate. The packages' thermal performance is significantly restricted. Second, to form strong interconnections, the bonding wires have to encircle a certain area, and thus have inherently high inductance (may exceed 10 nH [50]), which becomes problematic at high-frequency switching. Third, the unbalanced mechanical structure, i.e., wire bonds on the top of the die and substrate attachment on the bottom, may cause differential stress, and, hence, leads to failure at high temperature. To overcome these limitations, different packaging schemes have been investigated for high-temperature usage.

Aw *et al.* [51] and Woo *et al.* [52] present a high-temperature SiC DMOSFET power module with flip-chip packaging. As shown in Fig. 4, rather than using bond wires, the top connections from dies are made by copper clips, which not only have lower inductance than bonding wires, but also enable double-side cooling. This flip-chip module is able to withstand a 220 °C 500-h storage test. Sugawara *et al.* [53] present a 150 °C-rated 3.1-kV 600-A SiC diode module using press-pack packaging, whose conceptual drawing is given in Fig. 5. As shown, the module has symmetrical structure on top and bottom. It thereby has smaller

TABLE II
SUMMARY OF PUBLISHED HIGH-TEMPERATURE POWER SEMICONDUCTOR MODULES USING WIRE-BONDING SCHEME

| Reference No. | [44] [45] | [46] | [47] | [48] |
|---|---|---|---|---|
| Year of publication | 2006 | 2009 | 2011 | 2012 |
| Type | Full bridge | Half bridge | Three phase half bridge | Half bridge |
| Max. tested temperature | 250 °C ambient (Tested under 200Vdc, 176W ) | 250 °C junction (Tested under 300Vdc, 20kW) | 200 °C ambient (Under double pulse test) | 200 °C ambient (Under double pulse test) |
| Dies of each switching element | Cree SiC 4A 600V SBD×4 (parallel) SiCED SiC 5A 1000V JFET×4 (parallel) | Rohm SiC 30A 1200V DMOSFET×8 (parallel) | SiCED SiC 2.7mm×2.7mm 1200V SBD×2 (parallel) SiCED SiC 4.17mm×4.17mm 25A 1200V JFET×4 (parallel) | SiC 2.4mm×4.8mm 20A 1200V MOSFET×4 (parallel) |
| Solder | Pb-In solder (melt at 310 °C) | Not given | Not given | Not given |
| Substrate | DBC with 25 mils AlN substrate and 12 mils Nickel plated copper | DBC AlN substrate and Nickel plated copper | DBC $Si_3N_4$ substrate | DBA substrate (ceramic material not given) |
| Base plate | MMC made of AlSiC | MMC made of 80% Cu and 20% Mo | Not given | Copper |
| Bond wire | Not given | Al wire | 8mil Al wire | Al wire |
| Encapsulant | Not given | Not given | Not given | Nanotec-resin KA100 |
| Case | Not given | Polyamide injection molded plastic | Not given | Not given |

No, number; max., maximum; SBD, Schottky barrier diode; DBA, direct bond aluminum.

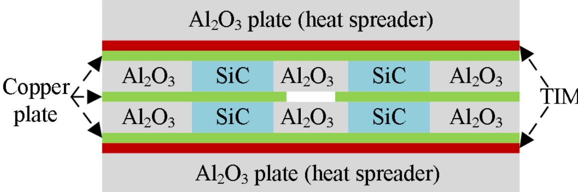


Fig. 6. Conceptual drawing of the 250 °C-rated planar module presented in [54], [55] (rectifier with four 1200-V, 50-A SiC Schottky barrier diodes).

differential mechanical stress than wire bonding packages. Both the top and bottom pads of dies are attached to electrodes with only a thin layer of molybdenum in between. The module thus has double-side cooling as well. In experiments, the forward characteristics (up to 800 A) of the diode module is measured at up to 150 °C ambient temperature. Valdez-Nava *et al.* [54] and Koyanagi *et al.* [56] present a bridge-rectifier power module with multilayer planar structure. As shown in Fig. 6, the module does not require any soldering, sintering, or bonding process. The pads of SiC diode dies are directly attached to copper plates, which also served as leads. Only vertical mechanical pressure is used to assure electrical connection. This rectifier module is tested under 700-V (RMS) 2-mA (RMS) input, at up to 250 °C ambient temperature. Yin *et al.* [56] introduce a ceramic-embedded SiC diode module, whose forward (forward current up to 3 A) and reverse characteristics (reverse voltage up to 600 V) are tested up to 236 °C ambient temperature. As shown in Fig. 7, the die pads are metalized to form a Cr layer, which is then directly bonded to the external copper layer forming circuit connection. According to the simulations presented in [56], the proposed structure can reduce thermally induced stress on die by 74.8% compared to wire bonding packages. The embedded module also allows double-side cooling.

## C. Magnetic Components

Magnetic components, i.e., inductors and transformers, can commonly be found in power electronics converters. Inductors either buffer large current in power circuits, or reject noises in

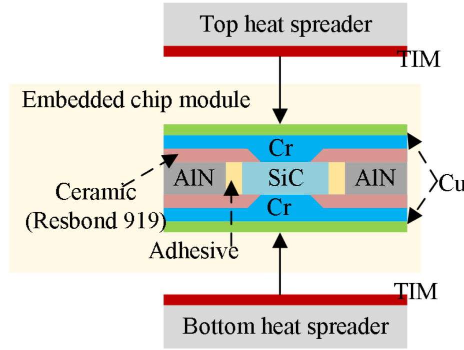


Fig. 7. Conceptual drawing of the 236 °C-rated embedded chip module (ECM) presented in [56] (the ECM has two SiC Schottky diodes, whose ratings are not given).

small signal circuits. Transformers provide galvanic isolation and impedance-matching in both power and signal circuits. Regardless of their various functionalities, all magnetic components are made of cores and windings, except those air-core magnetic components, which only have windings.

Conventional windings are made of film-insulated round magnet (enameled) wires. The qualification of temperature rating of such wires needs to comply with international standards such as ASTM D2307, i.e., Standard Test Method for Thermal Endurance of Film-Insulated Round Magnet Wire [57]. ASTM D2307 classifies magnet wires into seven thermal classes according to the maximum temperature that the magnet wire can be exposed to. The highest thermal class in ASTM D2307 is thermal class—240 °C, which states that the tested wire remains functional at 320 °C for 1 day, or 260 °C for 56 days. Other than magnet wires, PCB windings have also been widely used in magnetic components. Their performance at high temperature is included in the later section where high-temperature PCB is reviewed.

Compared to windings, cores are more likely the obstacle to operate magnetic components at high temperature. The Curie temperature $T_c$ sets the maximum temperature of a core. High-frequency (>10 kHz) power electronics converters usually

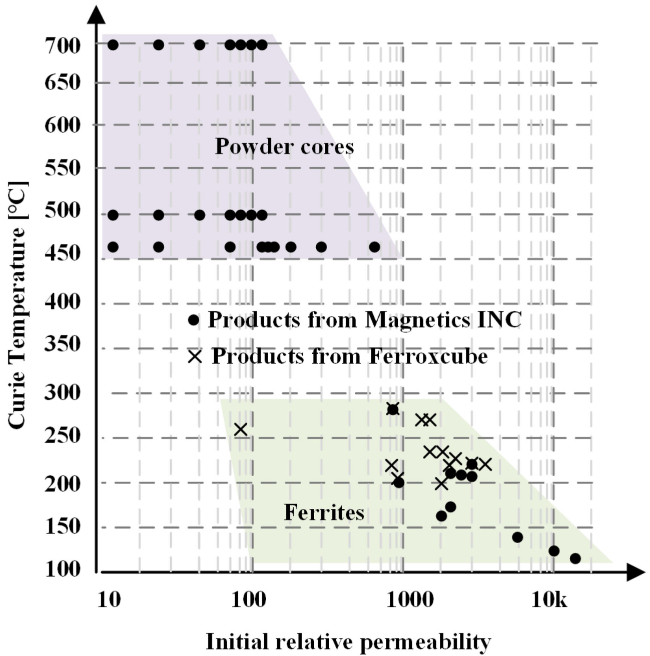


Fig. 8. Curie temperature and relative initial permeability of commercially available powder and ferrite cores from Magnetics INC and Ferroxcube (data gathered in August of 2021).

contain three kinds of cores, i.e., powder cores, ferrite cores, and tape wound. Depending on the material of alloy particles, powder cores have different Curie temperature with a range of 460–700 °C. Unlike powder cores, ferrite cores have relatively low Curie temperature. For example, MnZn ferrite cores, which are suitable for $< 1$ MHz switching, have Curie temperature of 210–240 °C. NiZn ferrite cores, which are suitable for $> 1$ MHz, have Curie temperature around 280 °C. Tape wound cores with cases are usually rated below 200 °C [58]. Fig. 8 gives the Curie temperature and relative initial permeability of commercially available powder and ferrite cores from Magnetics INC and Ferroxcube. As shown, there is a trade-off between the maximum operating temperature and the permeability of magnetic cores.

Besides the Curie temperature, the changing permeability and core loss with temperature make the design of magnetic components for wide temperature range difficult. The datasheet of a core material gives some information about the temperature drift of permeability and loss. For example, the datasheet of ferrite material N97 provides initial permeability vs. temperature ($-40$ °C $\sim$ Curie temperature), saturation flux density at 25 °C and 100 °C, and core loss versus temperature (25–140 °C) under 100-kHz magnetization with different maximum flux density (25, 50, 100, and 200 mT) [59]. To design magnetic components for wide temperature range, designers would prefer to have the B–H curves of cores measured at different temperatures and magnetizing conditions. However, such measurements or databases of magnetic cores are still hard to find.

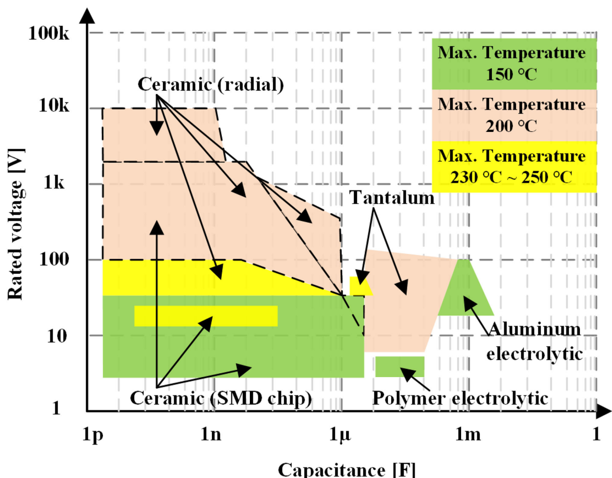


Fig. 9. Rated capacitance, rated voltage, and dielectric material of commercially available capacitors with maximum temperature rating $\geq 150$ °C from TDK, KEMET, and AVX (data gathered in June of 2021).

### *D. Capacitors*

In a power electronics converter, capacitors differ a lot in terms of capacitance (pF $\sim$ hundreds $\mu$ F) and voltage rating (a few volts to a few kV). To reduce cost and design complexity, designers prefer commercial products rather than customized capacitors. Fig. 9 gives the rated capacitance, rated voltage, and dielectric material of commercially available capacitors from TDK, KEMET, and AVX, with maximum temperature rating $\geq 150$ °C. As shown, capacitors with rated voltage $> 100$ V, capacitance $> 100$ $\mu$F, and temperature rating $> 150$ °C are hard to find. For $> 150$ °C operations, ceramic and tantalum capacitors should be the primary options to look at. For 150–200 °C operations, high-voltage (up to 10 kV), low-capacitance ($< 1$ $\mu$F) ceramic radial capacitors are available. Capacitors rated for $> 200$ °C operations all have rated voltage below 100 V.

Fig. 9 is made according to capacitors' rated capacitance and rated voltage, which are characterized at room temperature. Depending on capacitors' dielectric materials, capacitance and the maximum working voltage change differently with temperature. Ceramic capacitors are divided into two classes, i.e., EIA Class I and EIA Class II, according to the dielectric materials' temperature stability [60]. Class I ceramic dielectrics are temperature-stable. The commonly used Class I dielectric material is C0G (NP0). As an example, the maximum capacitance change of C0G ceramic capacitors from KEMET is 0.5% at 200 °C with reference to 25 °C. In comparison, KEMET X7R capacitors (Class II) have the maximum capacitance change of 15% at 125 °C with reference to 25 °C. However, Class I capacitors have lower volumetric efficiency than Class II capacitors. As shown in Fig. 9, as temperature goes up, the capacitance of available ceramic capacitors reduces. Tantalum capacitor is an option to have high capacitance ($> 1$ $\mu$F) at high-temperature ($> 150$ °C) and low-voltage ($< 100$ V) working conditions. The capacitance of tantalum capacitors does not drop with temperature. However, the maximum working voltage does. For example, the maximum

TABLE III
COMMERCIALLY AVAILABLE RESISTORS FROM VISHAY FOR > 175 °C OPERATIONS

| Compo -sition | Available packages | Max. temp. .[°C] | Resistance tolerance | Temperature coefficient -[ppm/°C] |
|---|---|---|---|---|
| Wire -wound coil | SMD | 275 | ±1% ∼ ±10% | ±20 ∼ ±400 |
| | TH | 350 | ±0.1% ∼ ±10% | ±20 ∼ ±1000 |
| | Chas | 450 | ±1% ∼ ±10% | ±20 ∼ ±400 |
| Thick film | SMD | 275 | ±1% ∼ ±10% | ±50 ∼ ±1100 |
| | TH | 175 | ±1% ∼ ±10% | ±200 ∼ ±900 |
| | Chas | 200 | ±1% ∼ ±10% | ±150 ∼ ±500 |
| Metal Oxide | TH | 230 | ±0.5% ∼ ±10% | ±50 ∼ ±400 |
| Thin film | SMD | 250 | ±0.02% ∼ ±1% | ±15 ∼ ±200 |
| Metal foil | SMD | 225 | ±0.01% ∼ ±5% | ±0.2 ∼ ±90 |
| | TH | 175 | ±0.005% ∼ ±1% | ±1 ∼ ±15 |
| Metal film | TH | 230 | ±0.1% ∼ ±10% | ±25 ∼ ±400 |
| Metal element | SMD | 275 | ±0.5% ∼ ±5% | ±110 ∼ ±3900 |
| | TH | 275 | ±1% ∼ ±5% | ±100 |

Max., maximum, temp., temperature; SMD, surface-mounting sevice; TH, through hole; chas, chassis mounting. Data gathered in June of 2021.

working voltage of KEMET T500 $MnO_2$ tantalum capacitors drops 40% at 200 °C with reference to 25 °C.

### E. Resistors

Resistors are fundamental components of power electronics converters. They are used in circuits that perform protection, current and voltage sensing, termination, signal processing, etc. For high-temperature operation, resistors' temperature rating is the basic requirement to fulfill. Additionally, the drift of resistance should be kept small over the working temperature range. Table III lists the maximum operating temperature, the resistance tolerance, and the temperature coefficient of resistors manufactured by Vishay. As shown, resistors' temperature rating and temperature drift mainly depend on the composition. Metal foil resistors offer the highest precision. However, their temperature rating is the lowest (< 225 °C). Thin-film resistors have moderate precision and higher maximum operating temperature (250 °C) than metal foil resistors. The remaining types of resistors have reduced precision, but increased temperature rating, and hence, high reliability under overload conditions.

### F. Gate Drivers

The majority of commercially available gate drivers are based on Si CMOS process, whose junction leakage current increases significantly once the junction temperature goes above 125 °C. The recommended maximum junction temperature of these Si-based gate drivers are 150 °C [62] [63]. Silicon-on-insulator (SOI) process, which has an oxide layer to reduce junction leakage current, offers a way to fabricate gate drivers for 150–225 °C operation [64]–[67]. CISSOID produces gate drivers that allow the maximum junction temperature to be 225 °C [67]. Gate drivers or gate-drive circuits for > 225 °C operations are mainly laboratory researches. And the majority of them are based on SiC process. Lamichhane *et al.* [69] present a gate driver IC based on SiC NMOS process. In the experiment, the gate driver dies can output 500-kHz, 30-V, and 50% duty-ratio square wave with 3-A peak source and sink current. The maximum temperature

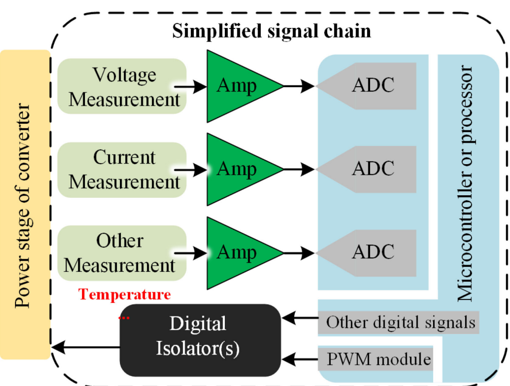


Fig. 10. Simplified signal chain of power electronics converters. Amp, amplifier; ADC, analog-to-digital converter; PWM, pulsewidth modulation.

on die during tests is 420 °C. However, the working conditions of the IC at 420 °C die temperature are not specified in [69]. Kargarrazi *et al.* [70] present a gate driver IC based on SiC bipolar technology. In experiments, the IC can robustly drive SCT2280KE (1.2-kV, 14-A SiC MOSFET) with 60-kHz, 20-V, and 50% duty-ratio square wave at up to 500 °C die temperature. Barlow *et al.* [72] present a gate driver IC based on SiC CMOS process. In experiments, the IC drives C3M0065090D (900-V, 36-A SiC MOSFET) with 15-V square wave (frequency and duty ratio are not specified) at up to 530 °C die temperature.

An alternative to gate driver ICs operating at 150–200 °C is gate drive circuits built with discrete components [72], [73]. These gate drive circuits usually have relatively large footprints and propagation delays compared to their IC counterparts. However, they use commercially available Si-based discrete transistors and diodes, which result in cheap solutions. The 225 °C rated gate driver ICs from CISSOID cost around 1600$per unit. In comparison, a 175 °C rated signal transistor from Nexperia cost < 1$. Moreover, with proper circuit design, gate drive circuits using discrete components can have comparable propagation delay to gate driver ICs [74].

### G. Signal Circuits

A typical signal chain of power electronics converters is sketched in Fig. 10. As shown, it mainly includes current and voltage measurement circuits, signal processing circuits, digital isolators, and microcontrollers or processors. These signal circuits need to operate reliably at high temperature as well.

A voltage measurement circuit is usually a resistor divider, whose accuracy and reliability depend on resistors chosen. As shown in Table III, metal foil and thin film resistors offer relatively high precision and low temperature drift. However, these two kinds of resistors are only rated up to 250 °C. Commercially available high-precision resistors that can operate reliably at > 250 °C are still few to find.

Current is usually measured by either shunt resistors or Hall effect current sensors [75]. Like voltage dividers, shunt-based current measurements require high-precision resistors, and hence can work up to 250 °C [76]. Hall effect current sensors inherently isolate amplifier circuits and microcontroller(s) from

power stage. However, commercially available Hall effect current sensor ICs have maximum operating ambient temperature of 150 °C [77]. Wrzecionko *et al.* [78] present an isolated dc and ac current measurement based on a saturated current transformer. The experimental setup is able to measure dc and ac sinusoidal current up to 50 A and 1 kHz at 250 °C ambient temperature with relative error of 2.6%. As a reference, the 150 °C-rated Hall effect sensor manufactured by ALLEGRO microsystems can measure up to 133 A with bandwidth from dc to 400 kHz and maximum total error of 1.75% [77]. Accurate current measurement solutions at $>$ 250 °C are still few to find.

Signal processing circuits are mainly composed of operational amplifiers (Op Amp), instrumentation amplifiers (In Amp), and voltage references. Like gate driver ICs, the majority of commercially available amplifier and voltage reference ICs are based on Si CMOS process, and are specified for maximum operating temperature of 125–150 °C. SOI process has been utilized by IC manufacturers to extend the temperature rating of their products. Analog devices produce amplifier (both Op Amp and In Amp) and voltage reference ICs that have predicted life time of 1000 h at 210 °C operating temperature [79]. CISSOID produces ceramic-packaged amplifier and voltage reference ICs that can operate up to 225 °C [80]. XREL semiconductor produces SOI-based voltage reference ICs that can operate up to 230 °C [81]. Amplifier and voltage reference ICs for $>$ 230 °C operation are mainly laboratory researches. Fraunhofer Institute for Integrated Systems and Device Technology has been developing 4H-SiC-based amplifiers that can operate up to 300 °C [82].

Digital isolators are sometimes needed in the signal chain of power electronics converters. Usually, signals are transferred through an isolation barrier by one of the three methods: optical coupling, capacitive coupling, and magnetic coupling. Commercially available digital isolator ICs are specified for maximum operating temperature of 125–150 °C. XREL semiconductors provide isolated data transceiver that can work up to 230 °C [83]. However, the galvanic isolation is achieved using external pulse transformers. VDDTECH promises that its 175 °C-rated digital isolator IC IZL-100 will be available in the fourth quarter of 2021.

High-temperature microcontrollers (processors) are fortunately available, enabling digital control for power electronics converters in high-temperature environment. Texas Instruments, a leading manufacturer of standard temperature microcontrollers, produces ceramic-packaged digital signal controller (DSC) and digital signal processor (DSP) that can operate up to 210 °C case temperature [84], [85]. These high-temperature DSC and DSP have the same features [e.g., memory size, number of pulsewidth modulation (PWM) outputs, number of high-resolution PWM outputs, number of channel, and resolution of analog-to-digital converter (ADC), configuration of serial port peripherals] as their standard temperature equivalents. However, they have to operate with reduced clock frequency at high temperature. Other than Texas Instruments, TEKMOS, VORAGO Technologies, and RelChip also produce microcontrollers that can work up to 300 °C, however, with less functional blocks than the counterparts from Texas Instruments. For example, VA10800 from VORAGO does not have built-in ADC module. Designers thereby have to seek external ones. Among these commercially available high-temperature microcontrollers, the 200 °C-rated ones are based on Si CMOS process, and the 300 °C-rated ones are based on SOI process.

Note that, other than the maximum temperature rating, temperature drift of components needs to be considered in the circuit design as well. For example, at elevated temperature, the resistance of shunt resistors increases, the noise rejection of amplifiers reduces, the line regulation of voltage references increases, and the threshold voltage of digital isolators reduces. Details about the temperature drift of the previously mentioned high-temperature signal electronic components can be found in their datasheets, and are not covered by this article.

TABLE IV
AGING OF FR4 MATERIAL R1755-V AND POLYMIDE ARLON 85 [87]

| Material | Temp. | Exposing time | Weight loss |
|---|---|---|---|
| R1755-V | 230 °C | 24 h | 8% |
| R1755-V | 190 °C | 650 h | 5% |
| ARLON 85 | 250 °C | 24 h | 1.8% |
| ARLON 85 | 190 °C | 1000 h | 1% |

Temp., temperature.

### *H. Printed Circuit Boards and Solders*

Printed circuit boards (PCBs), which holds together all of the components and circuits discussed above, are layer(s) of copper laminated onto or between layer(s) of nonconductive substrates. The operating temperature of PCBs needs to be lower than the glass transition temperature $T_g$ of substrates. Otherwise, delamination of PCB may occur. Protecting substrates from oxidation is important as well to increase life time of PCBs operating at high temperature [86]. The commonly used substrate materials for 150–200 °C operation is high $T_g$ FR4 (such as ISOLA IS410 and Shengyi S1000-2, both $T_g = 180$ °C) and high $T_g$ polyimide (such as ARLON 85 N, $T_g = 250$ °C). The aging of FR4 material Panasonic R1755-V ($T_g = 173$ °C) and polymide ARLON 85 N is characterized in [87], and is listed in Table IV. R1755-V exposed in air shows 8% weight loss after 24 h at 230 °C. ARLON 85 N exposed in air shows 1.8% weight loss after 24 h at 250 °C. Operating at 190 °C, R1755-V exposed in air shows 5% weight loss after 650 h, and ARLON 85 N exposed in air shows 1% weight loss after 1000 h. To increase the reliability and life time of PCBs at $>$ 200 °C, ceramic substrates such as $Al_2O_3$ and AlN can be used [88]. Currently, published work about using ceramic PCBs in power electronics converters is still few to find.

Solders join the metal leads and pads of components to PCBs. The melting temperature of solders are usually selected to be at least 40 °C higher than the maximum ambient temperature, considering the self heating of solder joints [2]. The majority of solders melting at 260–320 °C are Pb-based alloys. As mentioned, Pb posts threats to human health and environment. Therefore, industries have been calling for Pb-free high-temperature solders, among which gold-based and silver-based alloys are the most popular. Due to the high cost of gold and silver, Pb-based solders

still dominate applications having the maximum operating temperature below 250 °C. In addition to keeping the temperature of solder joints below the melting point, preventing the joints from cracking or deforming under wide temperature change and mechanical shock or vibration, which is usually encountered in high-temperature applications, is important as well. Some international standards, such as IPC-A-610, classify the quality of electronic component assembly, which includes forming solder joints with high mechanical stability [89]. The highest criteria of standard electronics assembly, such as IPC-A-610 Class 3, is usually referred as the minimum which high-temperature electronics assembly has to comply with. Currently, there is not any standards regulating the quality of assembling components for high-temperature usage. Manufacturers of high-temperature electronic equipment usually set up their own quality requirement based on field trials.

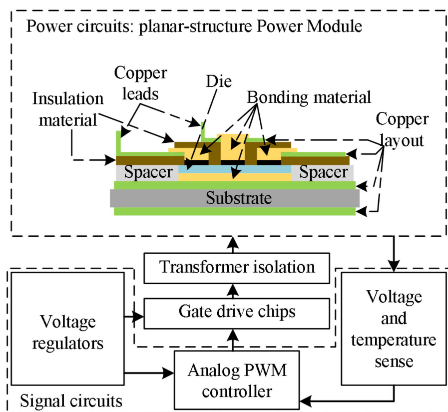


Fig. 11. Block diagram of the ac–dc converter presented in [90].

### *I. Other Components*

The high-temperature behaviors of other components such as connectors and heat sinks are not reviewed in this section. Because these parts are usually customized in high-temperature applications, they will be discussed in Section III, where individual high-temperature power electronics converters are reviewed.

## III. Converters Working at High Temperature

As mentioned, operating power electronics converters at high temperature is a systematic issue. All of the components discussed in Section II need to operate reliably. The temperature limitation and design challenges set by individual components are summarized as follows.

1) Semiconductor materials, such as SiC and GaN, can function at $> 500$ °C. However, the unavailability of encapsulation materials that are thermally stable at $> 250$ °C set the maximum operating temperature of packaged power semiconductor devices at 250 °C (refer to Section II-A and B for details).
2) Commercially available capacitors have temperature rating $< 250$ °C. Commercially available ferrite materials with Curie temperature higher than 250 °C all have relative permeability below 800, and are suitable for $>1$ MHz magnetizing frequency. High-precision resistors have temperature rating $< 225$ °C. Due the low capacitance of high-temperature capacitors, and the low permeability of high-temperature ferrites, the higher the operating temperature, the higher the switching frequency has to be. Therefore, to allow high-frequency operation, achieving zero voltage switching (ZVS) and reducing parasitics of layout are important (refer to Sections II-C, II-D, and II-E for details).
3) Commercially available gate driver ICs and other signal ICs (comparators, inverters, flip-flops, etc.) allow maximum junction temperature of 225 °C (refer to Section II-F and G for details).
4) Life time of PCBs reduces drastically at $> 250$ °C. Commonly used high-temperature solders are recommended for usage in $< 250$ °C operating temperature (refer to Section II-H for details).

Considering these temperature limitations and the self-heating of individual components, the maximum ambient temperature of power electronics converters is in the range of 210–240 °C, depending on system complexity. Therefore, in this article, the high end of the scale of high-(ambient)-temperature is set at 240 °C. The low end of the scale is set to be 150 °C because 150 °C is the point above which designers use components and assembly method different from norm of standard-temperature electronics [2].

The following of this section reviews power electronics converters, of which either the power circuits or the control circuits are designed and tested at the maximum-ambient-temperature ranging between 150 and 240 °C. The review of each converter starts by introducing the selected components and materials, in the same order as discussing high-temperature components and materials in Section II. Key experimental results are analyzed to reflect the efficacy of component–or material—selection and assembly methods. This section ends by summarizing the challenges of designing high-temperature power electronics converters from a system point of view.

### *A. AC–DC Converters*

Wang *et al.* [90] present the detailed design process and tests of a three-phase ac–dc converter, whose signal circuits and gate drive circuits can operate at ambient temperature up to 150 °C. The block diagram of the converter is given in Fig. 11. As shown, the power semiconductors are custom-designed planar-structure power modules, which, compared with traditional wire-bonding (shown in Fig. 2) structure, has smaller footprint, more flexible layout, less parasitic inductance, and double-side cooling capability. The gate signals are generated by commercially available gate drive chips, then isolated by custom-designed pulse transformers, and finally drive the power modules. The PWM signals are generated from a commercially available analog PWM controller. The output voltage is sensed for control and protection purposes. The die temperature is sensed through a type T thermocouple. The components and materials used to

TABLE V
SUMMARY OF MATERIALS AND COMPONENTS USED IN POWER ELECTRONICS CONVERTERS WITH THE MAXIMUM AMBIENT-TEMPERATURE RATED BETWEEN 150 AND 240 °C

| | Reference No. | [89] | [90] [91] | [92] | [93] [94] | [96] | [98] |
|---|---|---|---|---|---|---|---|
| | Year of publication | 2013 | 2016,2018 | 1997 | 2004,2005 | 2007 | 2013 |
| Converter specification | Conversion | AC-DC | DC-AC | DC-DC | DC-DC | DC-DC | DC-DC |
| | Topology | Three-phase diode rectifier | Three-phase inverter | Phase-shifted full-bridge | Boost | Forward | Interleaved boost |
| | Power rating | 1.4 kW | 30 kVA | 0.5 kW | 2 kW | 180W | 2 kW |
| | Input voltage [V] | 100 (rms,ac) | 300 (dc) | 28 (dc) | 270 (dc) | 270 (dc) | 100 (dc) |
| | Output voltage [V] | 270 (dc) | 97 (rms,ac) | 42 (dc) | 500 (dc) | 28 (dc) | 270 (dc) |
| | Switching frequency [kHz] | 30 | 10 | 25 | 40 | 100 | 74 |
| | Dimension | ∼16.5 cm×14 cm ×3.5 cm | Not given | Not given | Not given | Not given | Not given |
| | Weight [g] | 277 w/o heat sinks | Not given | Not given | Not given | Not given | Not given |
| | Max. ambient temp. of power circuits [°C] | 25 | 180 | 200 | 196 | 200 | 200 |
| | Max. junction temp. of power circuits [°C] | 250 | 150 | 212 | Not given | Not given | Not given |
| | Max. ambient temp. of gate drivers [°C] | 150 | 180 | 25 | 25 | 25 | 25 |
| | Max. ambient temp. of signal circuits [°C] | 150 | 25 | 25 | 25 | 25 | 25 |
| Power semiconductors | | Custom-designed power module | Cree power module CAS300M12BM2 | Si MOSFET-IR-F044 Si diode-MU-R5015 | Si MOSFET-IRF-P27N60K SiC diode-CS-D10060A | SiC BJT [95] SiC diode CS-D10060 and-CSD20030 | SiC JFET-SJEP120R125 SiC diode-CSD20030 |
| Structure of power module packaging | | Planar (Fig. 11) | Not given | N/A | N/A | N/A | N/A |
| Power module packaging details | Switch | SiCed SiC JFET 1200 V,5 A 3 mm × 3 mm | Cree C2M MOSFET | N/A | N/A | N/A | N/A |
| | Diode | SiCed SiC Diode 1200 V,5 A 2.7 mm × 2.7 mm | Cree Z-Rec™ Diode | N/A | N/A | N/A | N/A |
| | Substrate | AlN DBC 25 mils AlN 8 mils Cu | AlN DBC | N/A | N/A | N/A | N/A |
| | Bonding material | Sintered nano Ag Processing temp. 275 °C | Not given | N/A | N/A | N/A | N/A |
| | Bond wire | N/A | Not given | N/A | N/A | N/A | N/A |
| | Base plate | Duralco 132 | Copper | N/A | N/A | N/A | N/A |
| | Case | No case | Not given | N/A | N/A | N/A | N/A |
| | Encapsulant or insulation | Epo-tek 600 | Not given | N/A | N/A | N/A | N/A |
| | Lead-frame | Not given | Not given | N/A | N/A | N/A | N/A |
| Magnetic components | | 4C65 (NiZn) - pulse transformer for gate drive | pulse transformer for gate drive material not given | Square permalloy-tape wound | MPP-55110 powder core for output inductor | X-perm [97] for transformer and inductor | X-perm [97] for output inductor |
| Capacitors | | Ceramic capa-citor, part numner not given | Ceramic X7R 46× SXP47C105KAA for each phase | Not given | Multilayer ce-ramic capa-citor (X7R) | Ceramic capa-citor (X7R and C0G) | Ceramic capa-citor (X7R) |
| Resistors | | Thick-film | Not given | Not given | Not given | Not given | Not given |
| Gate drivers | | CHT-HYPERION from Cissoid | Circuit with discrete transistors | UC3875 | Not given | TC4422A | TC4422A |
| Signal circuits | Controller | CHT-MAGMA from Cissoid | Not given | UC3875 | Not given | SG3525 | SG3525 |
| | Op-amps | CMT-OPA-PSOIC16 from Cissoid | Not given | Not given | Not given | Not given | Not given |
| | Current sense | N/A | Not given | Not given | Not given | Not given | Not given |
| Auxiliary power supplies | | CHT-LDOP-150 from Cissoid | N/A | Not given | Not given | Not given | Not given |
| PCB | | Rogers 4350 | Not given | Not given | Not given | FR-4 | Not given |
| Solders | | 98%Pb-5%Sn | Not given | Not given | Not given | 95Sn5Sb | 95Sn5Sb |
| Thermal dissipation | | Heat sink with forced convection | 007-MXQ01 plate with 50 °C coolant | Heat sink with natural convection | Heat sink with natural convection | Heat sink with natural convection | Heat sink with natural convection |

No., number; max., maximum; min., minimum; temp., temperature; N/A, not applicable; w/o, without.

package the power module, and the components used in signal circuits are listed in Table V.

In [90], the power module is tested at room temperature. Therefore, the reliability of the packaging method and materials at high ambient temperature is unknown. The signal and gate drive circuits are composed by ICs rated up to 225 °C junction temperature. Therefore, these logic circuits are expected to be functional at 150 °C ambient temperature. The missing information is their response to the temperature drifts of these ICs. Wang *et al.* [90] present the logic circuits' latency performance at ambient temperature ranges from −50 to 150 °C. The switching frequency changes from 30 to 35 kHz when temperature is increased from 25 to 150 °C. The slew rate of the gate signals increases with temperature as well. It would be more informative if [90] could measure the power consumption of gate drive circuits at different ambient temperatures, as this

information can help specify the design of auxiliary power supplies.

### *B. DC–AC Converters*

Qi *et al.* [91] and Qi *et al.* [92] present the design and test of a three-phase inverter, whose power circuits and gate drive circuits can operate at ambient temperature up to 180 °C. The components used and converter specifications are listed in Table V. The power circuits are commercially available SiC power modules with the maximum junction temperature rated at 150 °C. To safely operate the power modules at 180 °C ambient temperature, cooling plate with 50 °C coolant is attached to the base plate of the power modules. Therefore, the power module itself is not designed for high temperature. However, the custom-designed gate drive circuit, which is built with cheap high-temperature Si transistors and only uses natural cooling, is rated up to 180 °C ambient temperature. The developed dc–ac converter system has controllers and voltage and current sensors. And they are room-temperature rated since the application, which is not specified, does not require these signal circuits to operate in a high-temperature environment. The converter does not have auxiliary power supplies.

The prototype presented in [91] and [92] is tested at 180 °C ambient temperature. Processing 31 kVA power, the power modules have 85 °C on the base plates. With calculated 300 W power loss generated from the power modules, the junction temperature of the power semiconductor dies is estimated to be 90 °C. The latency and power consumption of the custom-designed gate drive circuit is characterized at 25–180 °C ambient temperature. Driving a dummy load (5 Ω resistor in series with a 10-nF capacitor, which is close to the 11.7 nF input capacitance of the CAS300M12BM2 power module) with 10 kHz 50% duty-ratio +19 V/−5 V square wave, the gate drive circuit has less than 7% change in rise and fall time, less than 25% change in propagation delays, and less than 7% change in power consumption, when ambient temperature is increased from 25 to 180 °C.

### *C. DC–DC Converters*

Nelms and Johnson [93] present a phase-shifted full-bridge dc–dc converter, whose full-bridge (excluding the gate drivers) and isolation transformer are tested up to 200 °C ambient temperature. The specification and components of the converter are given in Table V. At the time when [93] was published, SiC power devices were not commercially available. The full-bridge is made by Si MOSFETs and Si diodes, which are not recommended by manufacturers to operate at 200 °C ambient temperature. Therefore, the MOSFETs and the diodes are characterized at 200 °C ambient temperature before the design of the converter. When the temperature is increased from 25 to 200 °C, the MOSFET's ON resistance is doubled, the MOSFET's leakage current increases from 1 nA to 1 mA, the MOSFET's gate threshold voltage decreases by 30%, the diode's leakage current increases from 100 nA to 1 mA, and the diode's forward voltage drops 25%. Although having these temperature drift in power semiconductor devices, the efficiency of the converter is not affected by ambient temperature. The measured efficiency of the converter operating at full power only drops from 86.1 to 85.4% when temperature is increased from 20 to 200 °C. The converter design strategy to cope with the temperature drift of components is not provided in [93]. The lifetime of the full-bridge and the transformer operating at 200 °C ambient temperature is tested and determined to be 3500 h. It would be more appreciated if the thermal design and the assembly method were discussed.

Ray *et al.* [94] and Ray *et al.* [95] present the detailed design and test of a boost converter, whose power stage can operate at 196 °C ambient temperature safely. The specification and component list of the prototype are given in Table V. Power stages with different combinations of power semiconductor devices are tested. The Si IGBT and Si diode combination has the lowest operating temperature. It fails at 110 °C ambient temperature. The turn-OFF time of the IGBT at 100 °C ambient temperature is 2.5 times of that at 30 °C. As a result, the turn-OFF loss of the IGBT increases significantly with temperature. With the measured waveform, the turn-OFF loss of Si IGBT and Si diode combination at 105 °C ambient temperature is three times of that at 30 °C. Changing the Si diode to SiC diode decreases the turn-OFF loss at 105 °C by 30%, which allows the Si IGBT and SiC diode combination to operate up to 120 °C ambient temperature. Replacing the Si IGBT with Si MOSFET reduces the turn-OFF loss at 30 °C by a factor of 3. Since the turn-OFF loss contributes the most part of the loss of the power stage, the operating temperature of both the Si MOSFET and Si diode combination and the the Si MOSFET and SiC diode combination increases significantly. Both are above 190 °C. Between these two, the Si MOSFET and SiC diode combination can operate at higher ambient temperature, i.e., 196 °C, due to the low reverse-recovery charge of SiC diode, which reduces the reverse-recovery loss of the diode and the turn-ON loss of the MOSFET. Life time test of the boost converter is not reported.

One year after the publication of [94] and [95], SiC BJT is developed by Cree [96]. About two years later, a full-SiC forward converter, whose power stage is capable of operating at 200 °C ambient temperature, is reported in [97]. The specification and component list of the forward converter are given in Table V. A custom-designed ferrite material, namely X-perm, is used in both the transformer and output inductor [98]. This X-perm ferrite features $>$ 300 °C Curie temperature, and is specially designed to have the lowest core loss at 200 °C. As a reference, commercially available ferrite materials usually have the lowest core loss at around 80 °C. In experiments, the power stage, i.e., SiC BJT, SiC diodes, transformer, output inductor, input and output capacitors, safely works in a 200 °C environment. It would be better if a loss breakdown, as the authors did in [94] and [95], could be made for this forward converter. The forward converter fails shortly after the ambient temperature is increased to 215 °C. The cause of the failure is the cracked input capacitors made of X7R ceramic. Therefore, leakage current test of X7R ceramic capacitor and C0G ceramic capacitor is conducted in [97]. And it is found that the leakage current of X7R ceramic capacitor increases exponentially at temperature $>$ 175 °C, which would overheat the capacitor and finally lead to crack. In contrast, the C0G ceramic capacitor has stable leakage current up to 225 °C, where the test is stopped. Life time test of the forward converter is not reported.

A few years after the publication of [97], SiC JFET and SiC MOSFET become commercially available. Kosai *et al.* [99] report an interleaved boost converter built with SiC JFETs, whose power stage can operate at 200 °C ambient temperature. The specification and component list of the converter are given in Table V. Compared to the components of the forward converter in [97], the interleaved boost converter in [99] replaces SiC BJT with SiC JFET, and keeps the selection of ferrite material, gate driver, controller, solder, and thermal dissipation setup.

### D. Challenges of Designing High-Temperature Power Electronics Converters

None of the converters reviewed in Sections III-A–C had both the power circuits and the control circuits rated at $> 150$ °C environment, although the device technologies, which have been reviewed in Section II, seem to allow $> 150$ °C operation of power electronics converters. The absence of publications about power electronics converters that can be entirely immersed into a $> 150$ °C environment indicates that designing a fully $> 150$ °C-rated converter might be very challenging.

The design of high-temperature power electronics converters is an iterative process that requires adequate experimental data of temperature drifts of all the components discussed in Section II. Due to the limited availability and the high cost of $> 200$ °C-rated components, designers sometimes have to use standard-temperature components above datasheet specifications. These standard-temperature components work at elevated temperature, but without guaranteed performance. The designers thereby have to characterize these components over temperature. For example, the temperature dependence of

1) MOSFETs' ON-resistance, threshold voltage, gate-to-source and drain-to-source leakage current, output capacitance, input capacitance, and Miller capacitance;
2) diodes' forward voltage drop, junction capacitance, leakage current, and breakdown voltage;
3) capacitors' leakage current, breakdown voltage, and capacitance;
4) magnetic cores' permeability, saturation flux density, and core loss;
5) gate drivers' propagation delay, rise and fall time, and power consumption.

In addition to characterizing the functionality, qualifying the reliability and lifetime of standard-temperature components at elevated temperature is necessary as well. However, there is not any standards for testing the life time and the reliability of electronic components operating in $> 150$ °C environment. Industries such as deep earth drilling usually define their own testing profile according to the field trials of their products. These processes of characterization and qualification are challenging, expensive, and time-consuming [2].

With the characterized component performance over temperature, designers can select components, and build and test prototypes. Based on the measured converter performance, the component selection might need adjustment. New prototypes are then built and tested. The new measurements are evaluated to decide if there is a need to further adjust the design. This iterative design-and-test procedure is time-consuming, but gives reliable design output. A possible way to reduce the development time is to use simulations. Simulation software such as LTspice, PSpice, Simulink, ANSYS, and COMSOL have been widely used in both industry and academia. These software allow designers to simulate converter performance over multiple physical domains, such as electrical, thermal, and mechanical. However, to have accurate simulation results, designers need to build device models using their data from component characterization. Such systematic simulations with very detailed component-level characteristics might become too memory-hungry and time-consuming to be advantageous to the design-and-test procedure. Therefore, another technical challenge of designing high-temperature power electronics converter is optimizing component selection within short development time.

## IV. Design of High-Temperature Converter With State-of-the-Art Standard-Temperature Components

The converters reviewed in Sections III-A–III-C were developed more than five years ago. Device technologies and design methodologies for power electronics have been continuously advancing during the past few years. However, it seems there is no recent publications about high-temperature power electronics converters. Therefore, this section will present the design of a 150 °C-rated dc–dc converter with state-of-the-art standard-temperature components. The design starts by characterizing standard-temperature components over temperature. The procedure of the characterizations is introduced in detail, to reflect on the discussions about device characterization in Section III-D. Then, an automated design flow is used to make component selection, as a reflection to the discussions about optimizing component-selection in Section III-D. Finally, the entire prototype, except the isolated power supplies for gate drivers and the digital controller, is tested in a 150 °C environment.

The dc–dc converter is a three-level neutral-point-clamped (TLNPC) converter with expected specifications as follows: input voltage $V_{in} = 1$–$1.5$ kV, output voltage $V_o = 600$ V, output power $P_o = 3$ kW, and ambient temperature of 150 °C.

### A. Characterization of Components

The performance of C0G ceramic capacitors and metal foil resistors operating in a 150 °C environment can be found from datasheet. The ICs in signal-processing circuits usually have power consumption around 10 mW. With 100 °C/W junction-to-case thermal resistance, it leads to less than 5 °C rise of junction temperature from environment. Using ICs specified with the maximum junction temperature of 150–175 °C may possibly give reliable operation of the signal processing circuits. The power switches, the power diodes, the ferrite materials, and the gate drivers, however, would have power consumption ranging from 100 mW to around 10 W, which leads to 10 °C rise of case temperature with respect to the environment temperature. With 150 °C ambient temperature, their case temperature may reach or even exceed 200 °C. In this design, a few commercially available standard-temperature power MOSFETs, ferrite materials, and gate drivers are characterized over temperature. Power diodes are not characterized because they rarely fail in previous tests. Life time

| SiC-Mfr.-1 | SiC-Mfr.-1 | SiC-Mfr.-2 | SiC-Mfr.-3 | SiC-Mfr.-4 |
|---|---|---|---|---|
| 2nd-Gen-1 | 3rd-Gen-1 | | | |
| 2nd-Gen-2 | 3rd-Gen-2 | device-1 | device-1 | |
| 2nd-Gen-3 | | | device-2 | device-1 |

Fig. 12. Illustration of characterized SiC MOSFETs.

and reliability cannot be tested in current development phase, because the associated testing profiles are not defined yet.

Nine SiC MOSFETs from four different manufacturers (SiC-Mfr.-1∼4) are selected for characterization. These SiC MOSFETs have the same 1.2 kV breakdown voltage, and the same TO-247 package. As illustrated in Fig. 12, among the nine MOSFETs, five are from SiC-Mfr.-1, one is from SiC-Mfr.-2, two are from SiC-Mfr.-3, and one is from SiC-Mfr.-4. Among the five MOSFETs from SiC-Mfr.-1, three belong to the second-generation (2nd Gen) device family, the rest two belong to the third-generation (3rd Gen) device family. The three 2nd Gen MOSFETs from SiC-Mfr.-1 have different current ratings. The current ratings of the rest six MOSFETs are close to that of the 2nd Gen MOSFETs from SiC-Mfr.-1. In Fig. 12, MOSFETs with similar current rating are placed in the same row. With this component selection, the temperature dependence of MOSFETs with different current ratings, belonging to different device generations, and from different manufacturers, can be compared, respectively. The test setup is the same as the one in [100] and [101], where a custom-made thermal chamber is used to heat up the MOSFETs, and a Keysight B1505 A Power Device Analyzer/Curve Tracer is used to measure the performance parameters introduced above.

As an example, Fig. 13 shows the temperature dependence of the ON resistance $R_{\mathrm{ds(on)}}$, the drain-to-source capacitance $C_{ds}$, and the gate-to-source capacitance $C_{gs}$ of seven of the selected MOSFETs. The remaining two MOSFETs from SiC-Mfr.-1 have high $R_{\mathrm{ds(on)}}$ and low $C_{gs}$ and $C_{ds}$. Therefore, their measurements are not plotted to maintain the resolution of Fig. 13. The plot shows the following.

1) The generation upgrade of SiC-Mfr.-1 reduces the temperature dependence of $R_{\mathrm{ds(on)}}$ by almost 100%, however, with the price of slightly increased $C_{gs}$ (by comparing SiC-Mfr.-1-2nd Gen-device-2 with SiC-Mfr.-1-3rd Gen-device-2).
2) Current rating does not change the temperature dependence of $R_{\mathrm{ds(on)}}$ of MOSFETs from the same manufacturer.
3) All of MOSFETs tested have stable $C_{gs}$ and $C_{ds}$ over temperature.
4) MOSFETs with the same current rating and drain-to-source breakdown voltage, but from different manufacturers, have around 10%–15% difference in $C_{gs}$, and 10%–70% difference in $C_{ds}$.

In a similar way, the gate threshold voltage $V_{th}$, the gate leakage current $I_g$, the drain-to-source leakage current $I_{d(\mathrm{off})}$, the body diode *i*–*v* characteristics, the third quadrant *i*–*v* characteristics, and the Miller capacitance $C_{gd}$ of all the nine MOSFETs are measured at ambient temperature ranging between 25 and 225 °C with 25 °C step size. These experimental data of MOSFETs' temperature dependence is used in the selection of gate

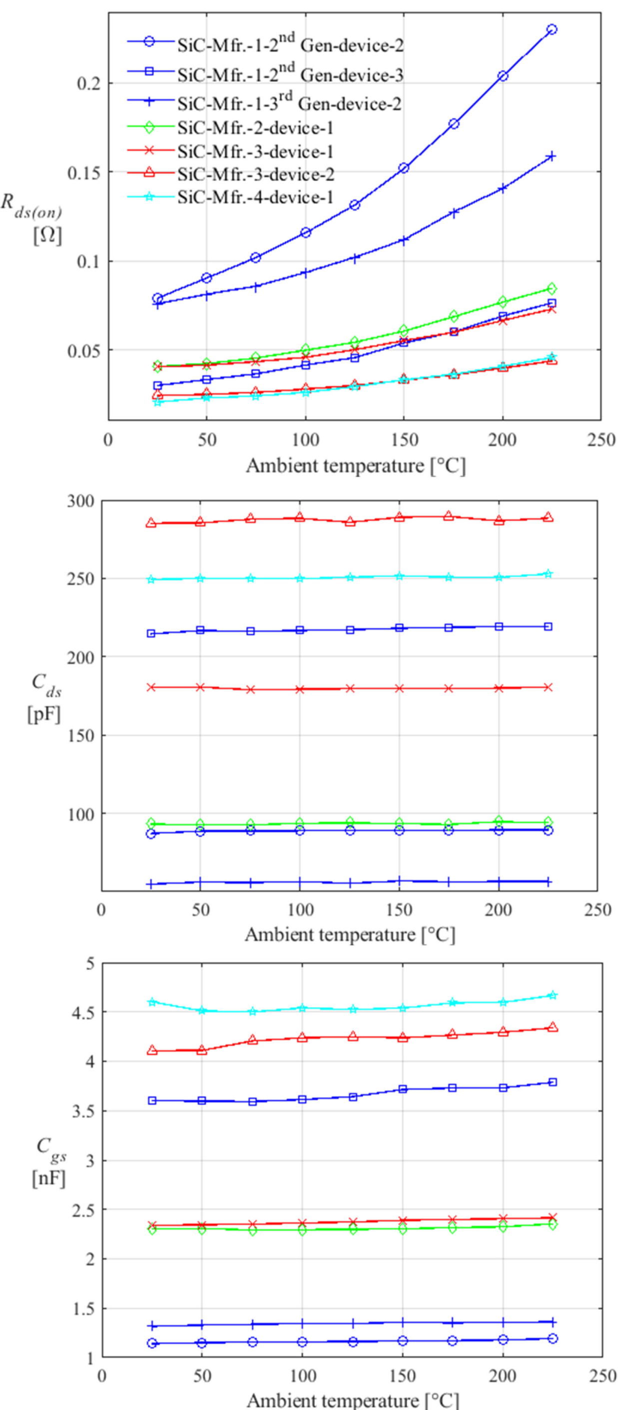


Fig. 13. Measured temperature dependence of $R_{\mathrm{ds(on)}}$, $C_{\mathrm{ds}}$, and $C_{\mathrm{gs}}$ of the selected MOSFETs (same legend for three plots).

drivers, the selection of switching frequency and dead time, the minimization of converter's conduction losses, and the design of ZVS.

Six gate drivers (GD 1–6) from different manufacturers are selected for characterization over temperature. The gate drivers are configured to generate 250-kHz, +15 V/−5 V square wave with 50% duty ratio. The output of the gate drivers is connected to load capacitors (1 and 2 nF, both are thermally stable C0G ceramic capacitors) through a 5-Ω resistor. The output condition

TABLE VI
CHARACTERIZED SOFT FERRITE MATERIALS AND THE TEST CONDITIONS

| Manufacturer | Material | Initial relative permeability at 25 °C | Magnetizing frequency in test [kHz] |
|---|---|---|---|
| Feri-Mfr.-1 | MTL-1 | 2200 | 100, 300, 500 |
| | MTL-2 | 3000 | 100, 300, 500 |
| | MTL-3 | 2300 | 100, 300, 500 |
| | MTL-4 | 1500 | 100, 300, 500, 1000 |
| | MTL-5 | 800 | 300, 500, 1000, 2000 |
| Feri-Mfr.-2 | MTL-1 | 2000 | 100, 150, 300, 500 |
| | MTL-2 | 3000 | 10, 100, 300, 500 |
| | MTL-3 | 1600 | 300, 500, 1000 |
| | MTL-4 | 900 | 100, 500, 1000, 2000, 3000 |
| | MTL-5 | 750 | 100, 500, 1000, 2000, 3000 |
| Feri-Mfr.-3 | MTL-1 | 2600 | 100, 300, 500 |
| | MTL-2 | 1100 | 300, 500, 1000 |
| | MTL-3 | 900 | 100, 500, 1000, 2000, 3000 |

and the load condition of the gate drivers are determined by the approximate range of switching frequency of the converter and the input capacitance of SiC MOSFET candidates. In the tests, the gate drivers are put into a thermal chamber. Their power consumption is logged through Siglent SDM3055 high-precision multimeters. Their latency are characterized through a RIGOL DS1054 oscilloscope. As an example, Fig. 14(a) shows the measured power consumption on driver side when the gate drivers output the specified 250 kHz square wave. As shown, the power consumption increases with temperature. However, some gate drivers are relatively thermally stable in terms of power consumption, such as GD-1 and GD-3. Fig. 14(a) also clearly indicates that the power consumption on driver side increases with load capacitance. However, the amount of increment of power consumption due to the doubled load capacitance is different from device to device. For example, the power consumption of GD-2 only increases 15% when the load capacitance is doubled, which means that GD-2 has high internal capacitance. The power consumption of GD 1–6 due to their internal capacitance is extracted, and is plotted in Fig. 14(b). Fig. 14(c) shows the temperature dependence of turn-OFF propagation delay. As shown, GD-1 has the lowest and thermally stable turn-OFF propagation delay. In a similar way, the static power consumption, the rise and fall time, and the turn-ON propagation delay of GD-1∼6 are measured. These experimental data of gate drivers' temperature dependence are used in the selection of MOSFETs, the selection of switching frequency, and the design of auxiliary power supplies for gate drivers.

As mentioned in Section II-C, for 200 °C operation, either ferrites or powder cores can be used. Compared to powder cores, ferrites have higher permeability and lower Curie temperature, i.e., 210–280 °C. When high permeability is required, ferrites are preferred. However, their performances such as amplitude permeability, saturation flux density, and core loss at $> 150$ °C are not specified in datasheets, which makes it risky to operate ferrites at 200 °C. Therefore, the temperature dependence of the B-H curves of a few commercial available ferrite materials are measured to support the converter design. The characterized ferrites and test conditions are summarized in Table VI. The B-H curve is extracted by a MADMIX power inductor measurement system. The cores are heated from 25 to 225 °C with 25 °C step size by the ATS-515-K-7 thermostream. The temperature

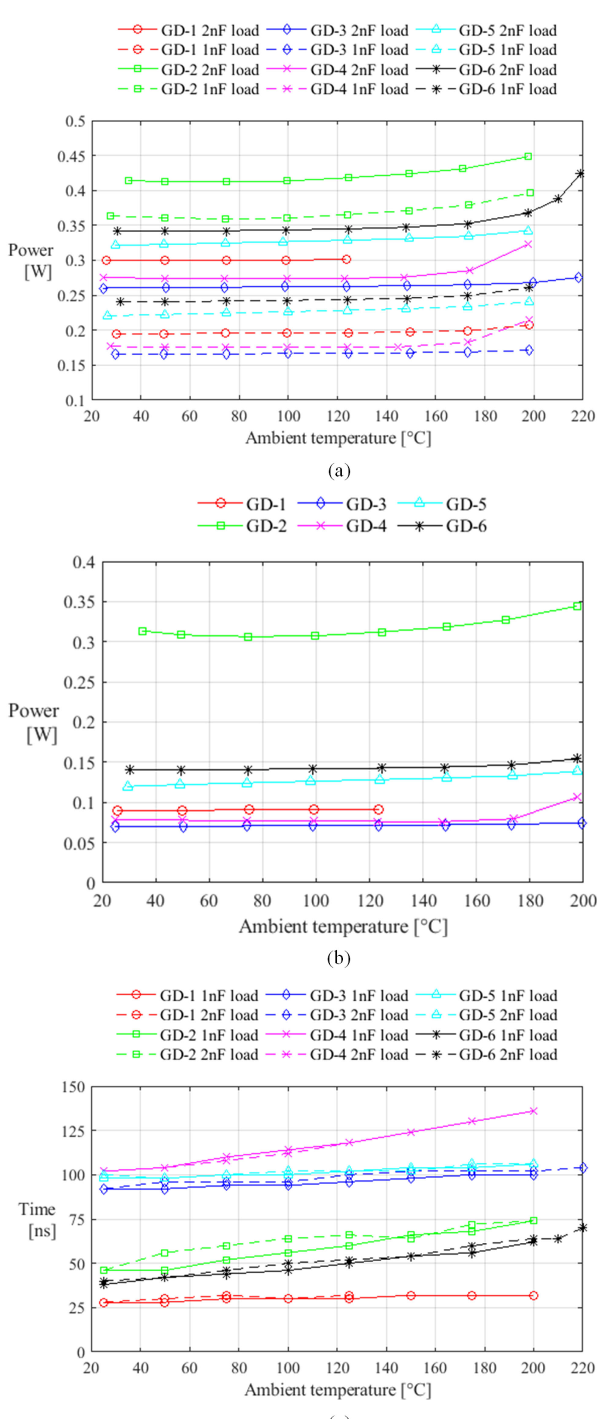


Fig. 14. Measured temperature dependence of power consumption and turn-OFF propagation delay of gate drivers @ 250 kHz, +15 V/−5 V, 50% duty-ratio square wave. (a) Power consumption on driver side at 250 KHz switching. (b) Power consumption on driver side at 250 KHz switching due to internal capacitance. (c) Turn-off propagation delay at 250kHz switching.

of the core is sensed by a K-type thermocouple and monitored by a AMPROBE 38XR-A multimeter. As an example, part of the characterizations of Feri-Mfr.-3-MTL-1 is given in Fig. 15. The following is shown in Fig. 15.

1) The saturation flux density $\mathbf{B}_s$ decreases with temperature. $\mathbf{B}_s$ at 222 °C is only a quarter of that at 25 °C. This

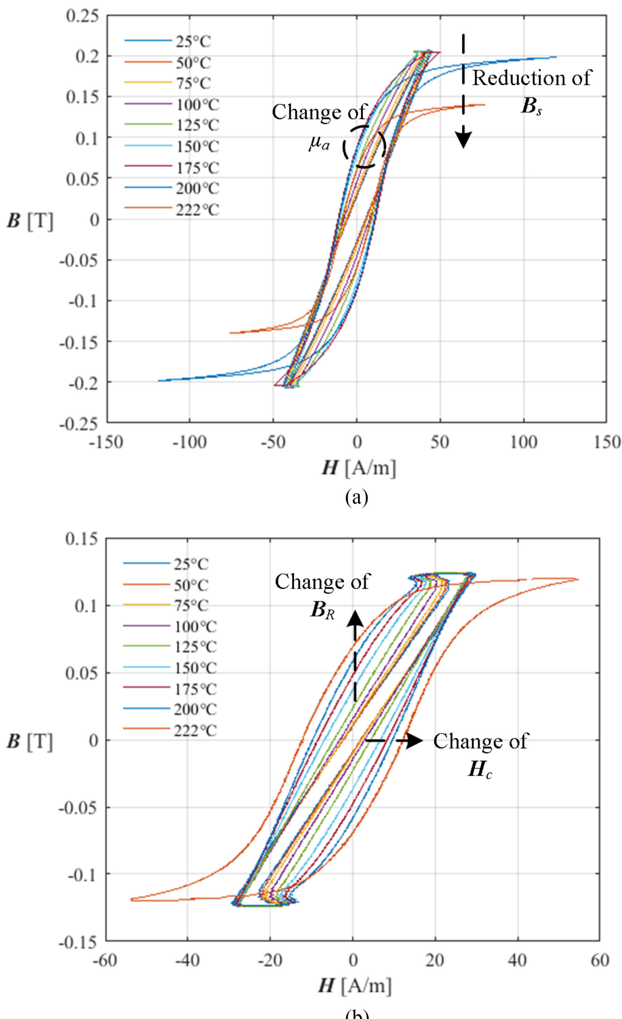


Fig. 15. Measured B-H curves of Feri-Mfr.-3-MTL-1 @ different ambient temperature and different magnetization frequencies. (a) 100 kHz magnetization frequency. (b) 300 kHz magnetization frequency.

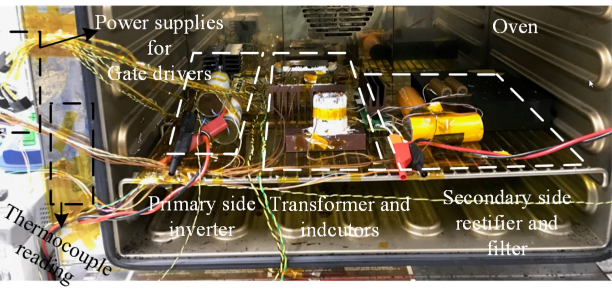


(a)

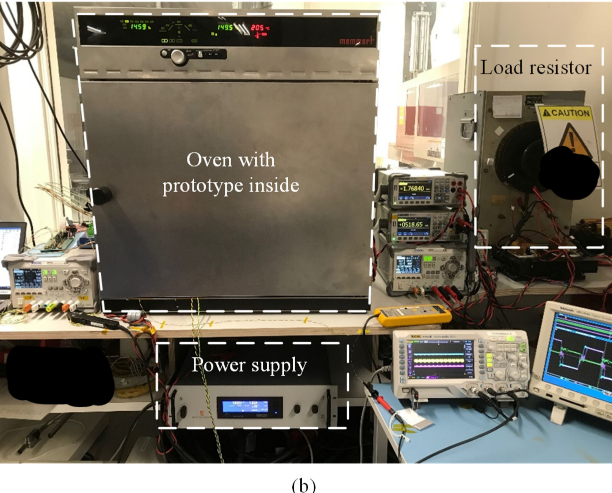


(b)

Fig. 16. TLNPC prototype and the test setup. (a) TLNPC prototype. (b) Test setup.

measurement indicates that Feri-Mfr.-3-MTL-1 can easily saturate at high temperature.

2) The amplitude permeability $\mu_a$ increases with temperature when temperature is below 175 °C, and decreases when temperature is above 175 °C. Note that the temperature dependence of $\mu_a$ differs from material to material. With the measured variation of $\mu_a$ over temperature, the temperature drift of inductance can be estimated.

3) The corrective field strength $\mathbf{H}_c$ and the remnant flux density $\mathbf{B}_R$ change with temperature, which indicates a changing core loss with temperature. The core loss density during each cycle of magnitization is calculated by integrating the flux density $\mathbf{B}$ over the field strength $\mathbf{H}$ using the measured B-H curves.

Similar characterizations are done to the remaining 12 ferrite materials. These experimental data of ferrites' temperature dependence are used in the selection of magnetic cores, and the optimization of circuit-level variables such as switching frequency, inductance, turns ratio of transformer, etc.

### B. Selection of Components

The process of component selection is actually a design flow, which evaluates the converter's performance, such as losses, voltage spikes, and realization of ZVS, under different component-selections. The design flow used combines analytical calculations and numerical simulations, and thus is more computationally efficient than design flows with pure numerical simulations. An improved topology model, the temperature characteristics of components, and the measurements from previous converter prototypes are incorporated into the design flow to guarantee the quality of design output. Moreover, the entire design flow is automated, and the program is published under an open-source license. The design flow has been presented in [102].

### C. Experiments

A TLNPC dc–dc converter prototype is built and tested in a 150 °C environment. The isolated power supplies for gate drivers and the digital controller are put outside of the oven. Fig. 16 gives pictures of the prototype and the test setup. Fig. 17 gives the measured efficiency of the prototype over temperature.

Compared to the expected specification, i.e., $V_{in} = 1$ kV $\sim$ 1.5 kV, $V_o = 600$ V, $P_o = 3$ kW, the prototype only operates up to $V_{in} = 1.1$ kV, $V_o = 520$ V, and $P_o = 1$ kW. The derated operation is due to the unexpected large power loss in the clamping diodes. The case temperature of some components of the prototype is

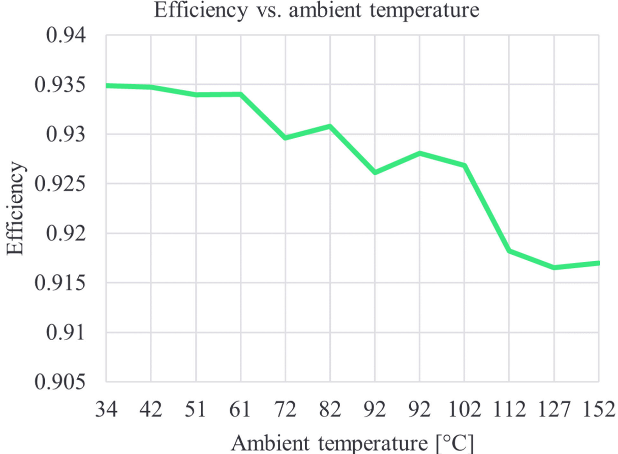


Fig. 17. TLNPC prototype efficiency vs. ambient temperature @ $V_{in} = 1$ kV, $V_o = 520$ V, $P_o = 1$ kW.

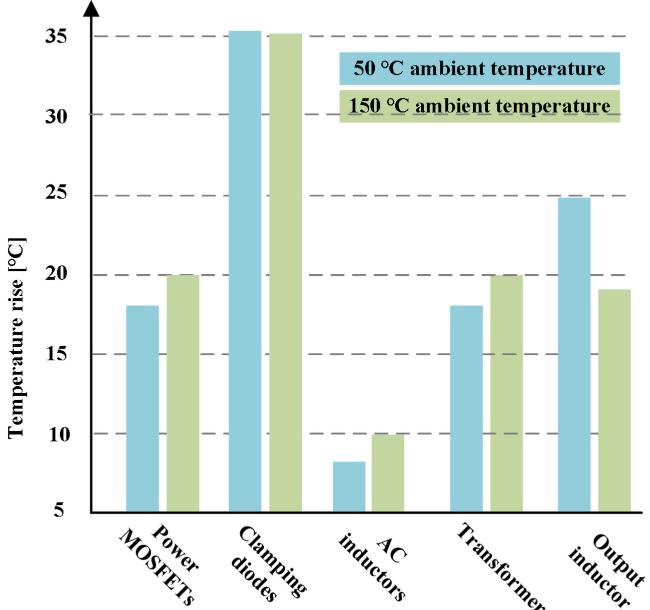


Fig. 18. Temperature rise of components after operating for 8 min @ $V_{in} = 1$ kV, $V_o = 520$ V, $P_o = 1$ kW, ambient temperature = 50 and 150 °C.

monitored by thermocouple. Fig. 18 gives the temperature rise of the monitored components after operating for 8 min. As shown, the measured temperature rise of the clamping diodes is around 35 °C, which is more than two times of the expected 15 °C temperature rise. This issue is not caused by the temperature drift of component characteristics, but the inadequate accuracy of modeling of the operation of the TLNPC converter. The extra 20 °C temperature rise will not kill the diodes under room temperature, but it might when the converter is immersed in a 150 °C environment. Therefore, since high-temperature power electronics converters only allow limited amount of temperature rise on the components, the tolerances of calculations in development phase have to be small, i.e., highly accurate models are needed.

The temperature breakdown also indicates potential improvements that can be made to the current design. For example, the temperature rise of the ac inductors is around 10 °C, which is lower than the expected 15–20 °C. Therefore, the ac inductors can be redesigned to be smaller.

Additionally, the temperature rise of components at different ambient temperature helps relate the temperature drift of individual components, which have been obtained from device characterization in Section IV-A, to their performance in actual circuit over temperature. For example, based on the characterization of the selected MOSFET, its $R_{\text{ds(on)}}$ should increase 54% when the ambient temperature is increased from 50 to 150 °C. However, the temperature rise of the MOSFET in experiments only increases 11% when the ambient temperature is increased from 50 to 150 °C. Some ideas for research can thereby be inspired from this observation. For instance, the case-to-ambient thermal resistance of the MOSFETs in the prototype may decrease with temperature; the temperature dependence of $R_{\text{ds(on)}}$ at in-circuit operation might be different to that at static characterization. Similar analysis can be made on the clamping diodes and the output inductor. The temperature rise of the clamping diodes does not change, indicating that their forward voltage remains unchanged. As we know, the forward voltage of a diode is the sum of the threshold voltage, which decreases with temperature, and the voltage drop due to internal resistance, which increases with temperature. In the tests, these temperature-dependences might have canceled out, and result in diode losses that are independent of temperature. The temperature rise of the output inductor decreases by around 7 °C. The reason for this is mainly the reduced core loss of MPP cores at 150 °C ambient temperature compared to that at 50 °C [103].

## V. Conclusion

Currently, there is only few publications about high-temperature power electronics converters and characteristics of components at high temperature, mainly because that the market size of applications using high-temperature converters is still small. The design and implementation of high-temperature converters hardly had any guidelines to reference to. A possible design procedure is to first characterize components over temperature. Then, an accurate model of the topology should be used or derived to design circuit parameters and select components. Finally, experimental verification should be done to check the efficacy of design, and to decide if there is a need to adjust. Because there is no standards regulating the test and qualification of components at high temperature, the components might still fail when operating in a converter although they had passed some self-defined qualification procedures. Therefore, the high-temperature qualification procedure of components changes from design to design, and usually needs modification after field trial of the converter prototypes.

In the future, if industries such as geothermal and commercial space travel continue expanding, the market size of high-temperature power electronics might grow. More researches about high-temperature converters can then be expected. The most essential researches will be $> 250$ °C-rated materials, such as encapsulants for packaging, dielectric materials for capacitors, ferrites, etc. These materials are the foundations of high-temperature converters. With more high-temperature

converters in the market, hopefully, there would be standards set for qualification of components and testing of converters. By following these standards, the design procedure of high-temperature converters might become less rigorous than now.

## REFERENCES


[1] J. Watson and G. Castro, "High-temperature electronics pose design and reliability challenges," *Analog Dialogue*, vol. 46, no. 2, pp. 3–9, Apr. 2012. [Online]. Available: https://www.analog.com/media/en/analog-dialogue/volume-46/number-2/articles/high-temperature-electronic-pose-design-challenges.pdf

[2] J. Watson and G. Castro "A review of high-temperature electronics technology and applications," *J. Mater. Sci.: Mater. Electron.*, vol. 26, pp. 9226–9235, 2015. [Online]. Available: https://doi.org/10.1007/s10854-015-3459-4

[3] R. W. Johnson, J. L. Evans, P. Jacobsen, J. R. Thompson, and M. Christopher, "The changing automotive environment: High-temperature electronics," *IEEE Trans. Electron. Packag. Manuf.*, vol. 27, no. 3, pp. 164–176, Jul. 2004.

[4] S. Lande, "Supply and demand for high temperature electronics," in *Proc. HITEN 3rd Eur. Conf. High Temp. Electron.*, 1999, pp. 133–135, doi: 10.1109/HITEN.1999.827477.

[5] R. F. Jurgens, "High-temperature electronics applications in space exploration," *IEEE Trans. Ind. Electron.*, vol. IE- 29, no. 2, pp. 107–111, May 1982.

[6] E. A. Kolawa, Y. Chen, M. M. Mojarradi, C. T. Weber, and D. J. Hunter, "A motor drive electronics assembly for Mars Curiosity Rover: An example of assembly qualification for extreme environments," in *Proc. IEEE Int. Rel. Phys. Symp.*, 2013, pp. 2E.2.1–2E.2.9, doi: 10.1109/IRPS.2013.6531963.

[7] P. L. Dreike, D. M. Fleetwood, D. B. King, D. C. Sprauer, and T. E. Zipperian, "An overview of high-temperature electronic device technologies and potential applications," *IEEE Trans. Compon., Packag., Manuf. Technol.: A.*, vol. 17, no. 4, pp. 594–609, Dec. 1994.

[8] C. D. Thurmond, "The standard thermodynamic functions for the formation of electrons and holes in Ge, Si, GaAs, and GaP," *J. Electrochem. Soc.*, vol. 122, 1975, Art. no. 1133.

[9] A. R. Hefner, R. Singh, J.-S. Lai, D. W. Berning, S. Bouche, and C. Chapuy, "SiC power diodes provide breakthrough performance for a wide range of applications," *IEEE Trans. Power Electron.*, vol. 16, no. 2, pp. 273–280, Mar. 2001.

[10] C. Raynaud, D. Tournier, H. Morel, and D. Planson, "Comparison of high voltage and high temperature performances of wide bandgap semiconductors for vertical power devices," *Diamond Related Mater.*, vol. 19, pp. 1–6, 2010.

[11] F. M. Shah, H. M. Xiao, R. Li, M. Awais, G. Zhou, and G. T. Bitew, "Comparative performance evaluation of temperature dependent characteristics and power converter using GaN, SiC and Si power devices," in *Proc. IEEE 12th Int. Conf. Compat., Power Electron. Power Eng.*, 2018, pp. 1–7, doi: 10.1109/CPE.2018.8372523.

[12] "NSM archive – Physical properties of semiconductors." [Online]. Available: http://www.ioffe.ru/SVA/NSM/Semicond/

[13] Y. P. Varshni, "Temperature dependence of the energy gap in semiconductors," *Physica*, vol. 34, no. 1, pp. 149–154, 1967, doi: 10.1016/0031-891490062-6.

[14] H. R. Philipp and E. A. Taft, *Silicon Carbide-A High Temperature Semiconductor*, J. R. O'Connor, and J. Smiltens, Eds. Oxford, U.K.: Pergamon Press, 1960, pp. 366–366.

[15] S. Petalas, S. Logothetidis, S. Boultadakis, M. Alouani, and J. M. Wills, "Optical and electronic-structure study of cubic and hexagonal GaN thin films," *Phys. Rev. B*, vol. 52, no. 11, pp. 8082–8091, 1995.

[16] H. J. McSkimin, "Measurement of elastic constants at low temperatures by means of ultrasonic waves-data for silicon and germanium single crystals, and for fused silica," *J. Appl. Phys.*, vol. 24, no. 8, pp. 988–997, 1953.

[17] F. J. Morin and J. P. Maita, "Electrical properties of silicon containing arsenic and boron," *Phys. Rev.*, vol. 96, no. 1 28–35, 1954.

[18] D. L. Barrett and R. B. Campbell, "Electron Mobility Measurements in SiC Polytypes," *J. Appl. Phys.*, vol. 38, no. 1, p. 53, 1967.

[19] R. Gaska *et al.*, "Electron transport in AlGaN-GaN heterostructures grown on 6H-SiC substrates," *Appl. Phys. Lett.*, vol. 72, no. 6, pp. 707–709, 1998.

[20] C. Jacoboni, C. Canali, G. Ottaviani, and A. A. Quaranta, "A review of some charge transport properties of silicon," *Solid State Electron.*, vol. 20, no. 2, pp. 77–89, 1977.

[21] C. J. Glassbrenner and G. A. Slack, "Thermal Conductivity of Silicon and Germanium from 3K to the Melting Point," *Phys. Rev.*, vol. 134, no. 4A, pp. A1058–A1069, 1964.

[22] D. Morelli, J. Hermans, C. Beetz, W. S. Woo, G. L. Harris, and C. Taylor, *Silicon Carbide and Related Materials* (Institute of Physics Conference Series N137), Bristol, Philadelphia: Institute of Physics Pub. Washington DC, 1993, pp. 313–316.

[23] R. Kucharski, T. Sochacki, B. Lucznik, and M. Bockowski, "Growth of bulk GaN crystals," *J. Appl. Phys.*, vol. 128, 2020, Art. no. 050902, doi:10.1063/5.0009900.

[24] B. Lu and T. Palacios, "High breakdown ($>$ 1500 V) AlGaN/GaN HEMTs by substrate-transfer technology," *IEEE Electron Device Lett.*, vol. 31, no. 9, pp. 951–953, Sep. 2010, doi: 10.1109/LED.2010.2052587.

[25] H. Lee, V. Smet, and R. Tummala, "A review of SiC power module packaging technologies: Challenges, advances, and emerging issues," *IEEE Trans. Emerg. Sel. Topics Power Electron.*, vol. 8, no. 1, pp. 239–255, Mar. 2020.

[26] V. R. Manikam and K. Y. Cheong, "Die attach materials for high temperature applications: A review," *IEEE Trans. Compon., Packag. Manuf. Technol.*, vol. 1, no. 4, pp. 457–478, Apr. 2011.

[27] F. Yu, J. Cui, Z. Zhou, K. Fang, R. W. Johnson, and M. C. Hamilton, "Reliability of Ag sintering for power semiconductor die attach in high-temperature applications," *IEEE Trans. Power Electron.*, vol. 32, no. 9, pp. 7083–7095, Sep. 2017.

[28] A. A. Bajwa, Y. Qin, R. Reiner, R. Quay, and J. Wilde, "Assembly and packaging technologies for high-temperature and high-power GaN devices," *IEEE Trans. Compon., Packag. Manuf. Technol.*, vol. 5, no. 10, pp. 1402–1416, Oct. 2015.

[29] Z. Lin and R. J. Yoon, "An AlN-based high temperature package for SiC devices: Materials and processing," in *Proc. Int. Symp. Adv. Packag. Mater.: Processes, Properties Interfaces*, 2005, vol. 2005, pp. 156–159.

[30] P. Ning *et al.*, "SiC wirebond multichip phase-leg module packaging design and testing for harsh environment," *IEEE Trans. Power Electron.*, vol. 25, no. 1, pp. 16–23, Jan. 2010.

[31] M. J. Palmer, R. W. Johnson, T. Autry, R. Aguirre, V. Lee, and J. D. Scofield, "Silicon carbide power modules for high-temperature applications," *IEEE Trans. Compon., Packag. Manuf. Technol.*, vol. 2, no. 2, pp. 208–216, Feb. 2012.

[32] T. G. Lei, J. N. Calata, K. D. T. Ngo, and G. Lu, "Effects of large-temperature cycling range on direct bond aluminum substrate," *IEEE Trans. Device Mater. Rel.*, vol. 9, no. 4, pp. 563–568, Dec. 2009.

[33] J. T. Benoit *et al.*, "Wire bond metallurgy for high temperature electronics," in *Proc. 4th Int. High Temp. Electron. Conf.*, 1998, pp. 109–113, doi: 10.1109/HITEC.1998.676770.

[34] Z. Chen, Y. Yao, D. Boroyevich, K. D. T. Ngo, P. Mattavelli, and K. Rajashekara, "A 1200-V, 60-A SiC mosfet multichip phase-leg module for high-temperature, high-frequency applications," *IEEE Trans. Power Electron.*, vol. 29, no. 5, pp. 2307–2320, May 2014.

[35] Z. Wang *et al.*, "A high temperature silicon carbide mosfet power module with integrated silicon-on-insulator-based gate drive," *IEEE Trans. Power Electron.*, vol. 30, no. 3, pp. 1432–1445, Mar. 2015, doi: 10.1109/TPEL.2014.2321174.

[36] H. A. Mustain, A. B. Lostetter, and W. D. Brown, "Evaluation of gold and aluminum wire bond performance for high temperature (500 /spl deg/C) silicon carbide (SiC) power modules," in *Proc. Electron. Compon. Technol.*, 2005, vol. 2, pp. 1623–1628, doi: 10.1109/ECTC.2005.1442008.

[37] L. Coppola, D. Huff, F. Wang, R. Burgos, and D. Boroyevich, "Survey on high-temperature packaging materials for SiC-based power electronics modules," in *Proc. IEEE Power Electron. Specialists Conf.*, 2007, pp. 2234–2240, doi: 10.1109/PESC.2007.4342356.

[38] CISSOID, "High temperature 1200 V/10 A silicon carbide MOSFET," CHT-NEPTUNE-1210 datasheet, *Version: 4.7*.

[39] H. Zhang, L. M. Tolbert, J. H. Han, M. S. Chinthavali, and F. Barlow, "18 kW three phase inverter system using hermetically sealed SiC phase-leg power modules," in *Proc. 25th Annu. IEEE Appl. Power Electron. Conf. Expo.*, 2010, pp. 1108–1112, doi: 10.1109/APEC.2010.5433365.

[40] Z. Cole *et al.*, "High temperature, wide bandgap full-bridge power modules for high frequency applications," in *Proc. IEEE Int. Workshop Integr. Power Packag.*, 2015, pp. 119–122, doi: 10.1109/IWIPP.2015.7295993.

[41] M. Locatelli *et al.*, "Evaluation of encapsulation materials for high-temperature power device packaging," *IEEE Trans. Power Electron.*, vol. 29, no. 5, pp. 2281–2288, May 2014.

[42] R. Khazaka, L. Mendizabal, D. Henry, and R. Hanna, "Survey of high-temperature reliability of power electronics packaging components," *IEEE Trans. Power Electron.*, vol. 30, no. 5, pp. 2456–2464, May 2015.
[43] Y. Yao, Z. Chen, G. Lu, D. Boroyevich, and K. D. T. Ngo, "Characterization of encapsulants for high-voltage, high-temperature power electronic packaging," in *Proc. 60th Electron. Compon. Technol. Conf.*, 2010, pp. 1834–1840, doi: 10.1109/ECTC.2010.5490712.
[44] L. Liu, D. Nam, B. Guo, J. Ewanchuk, R. Burgos, and G.-Q. Lu, "Glass for encapsulating high-temperature power modules," *IEEE J. Emerg. Sel. Topics Power Electron.*, vol. 9, no. 3, pp. 3725–3734, Jun. 2021, doi: 10.1109/JESTPE.2020.3004021.
[45] J. M. Homberger, E. Cilio, R. M. Schupbach, A. B. Lostetter, and H. A. Mantooth, "A high-temperature multichip power module (MCPM) inverter utilizing silicon carbide (SiC) and silicon on insulator (SOI) electronics," in *Proc. 37th IEEE Power Electron. Specialists Conf.*, 2006, pp. 1–7, doi: 10.1109/pesc.2006.1711732.
[46] E. Cilio, J. Hornberger, B. McPherson, R. Schupbach, and A. Lostetter, "Design and fabrication of a high temperature (250°C baseplate), high power density silicon carbide (SiC) multichip power module (MCPM) inverter," *Proc. IECON - 32nd Annu. Conf. IEEE Ind. Electron.*, 2006, pp. 1822–1827, doi: 10.1109/IECON.2006.347960.
[47] A. Lostetter *et al.*, "High-temperature silicon carbide and silicon on insulator based integrated power modules," in *Proc. IEEE Veh. Power Propulsion Conf.*, 2009, pp. 1032–1035, doi: 10.1109/VPPC.2009.5289735.
[48] F. Xu *et al.*, "High temperature packaging of 50 kW three-phase SiC power module," in *Proc. 8th Int. Conf. Power Electron.-Asia*, 2011, pp. 2427–2433, doi: 10.1109/ICPE.2011.5944718.
[49] T. Funaki, M. Sasagawa, and T. Nakamura, "Multi-chip SiC DMOSFET half-bridge power module for high temperature operation," in *Proc. 27th Annu. IEEE Appl. Power Electron. Conf. Expo.*, 2012, pp. 2525–2529, doi: 10.1109/APEC.2012.6166178.
[50] F. Hou *et al.*, "Review of packaging schemes for power module," *IEEE Trans. Emerg. Sel. Topics Power Electron.*, vol. 8, no. 1, pp. 223–238, Mar. 2020.
[51] J. L. Aw, B. Lin, H. H. Yuan, and D. R. M. Woo, "Process development and optimization for high temperature endurable flip chip interconnection in SiC high power module," in *Proc. IEEE 16th Electron. Packag. Technol. Conf.*, 2014, pp. 225–228, doi: 10.1109/EPTC.2014.7028357.
[52] D. R. M. Woo, H. H. Yuan, J. A. J. Li, L. J. Bum, and Z. Hengyun, "Miniaturized double side cooling packaging for high power 3 phase SiC inverter module with junction temperature over 220°C," in *Proc. IEEE 66th Electron. Compon. Technol. Conf.*, 2016, pp. 1190–1196, doi: 10.1109/ECTC.2016.396.
[53] Y. Sugawara *et al.*, "3 kV 600 A. 4H-SiC high temperature diode module," in *Proc. 14th Int. Symp. Power Semicond. Devices ICs*, 2002, pp. 245–248, doi: 10.1109/ISPSD.2002.1016217.
[54] Z. Valdez-Nava, M. Kozako, S. Dinculescu, I. Omura, M. Hikita, and T. Lebey, "Packaging of SiC-SBD for high temperature operation," in *Proc. 14th Int. Conf. Electron. Mater. Packag.*, 2012, pp. 1–4, doi: 10.1109/EMAP.2012.6507921.
[55] K. Koyanagi *et al.*, "Development of a new package for next generation power semiconductor devices: Toward high temperature and high voltage applications," in *Proc. IEEE 10th Int. Conf. Power Electron. Drive Syst.*, 2013, pp. 512–516, doi: 10.1109/PEDS.2013.6527072.
[56] J. Yin, Z. Liang, and J. D. van Wyk, "High temperature embedded SiC chip module (ECM) for power electronics applications," *IEEE Trans. Power Electron.*, vol. 22, no. 2, pp. 392–398, Mar. 2007.
[57] ASTM International, *D2307-07a(2013) Standard Test Method for Thermal Endurance of Film-Insulated Round Magnet Wire*. West Conshohocken, PA, USA: ASTM International, 2013, doi: 10.1520/D2307-07AR13.
[58] Magnetics, "Tape wound cores," *Product Catalog*, 2016.
[59] TDK, "SIFERRIT material N97," *Mater. Datasheet*, May 2017.
[60] EIA-198-1, Revision F., "Ceramic dielectric capacitors classes I, II, III, and IV - Part I: Characteristics and requirements," Nov. 2002.
[61] Vishay, "Vitreous wirewound power resistors," Datasheet [*Revision: Aug. 08, 2016*].
[62] Texas Instrum., "UCC21710-Q1 10-A source/sink reinforced isolated single channel gate driver for SiC/IGBT with active protection, isolated analog sensing and high-CMTI," UCC21710-Q1 Datasheet, 2019 [*Revised:* Dec. 2019].
[63] Analog Devices, "Single gate, adjustable slew rate, isolated gate driver, 3 A short-circuit (Ω)," ADuM4122 Datasheet, [Rev. 0].
[64] M. A. Huque, R. Vijayaraghavan, M. Zhang, B. J. Blalock, L. M. Tolbert, and S. K. Islam, "An SOI-based high-voltage, high-temperature gate-driver for SiC FET," in *Proc. IEEE Power Electron. Specialists Conf.*, 2007, pp. 1491–1495, doi: 10.1109/PESC.2007.4342215.
[65] K. E. Falahi, B. Allard, D. Tournier, and D. Bergogne, "Evaluation of commercial SOI driver performances while operated in extreme conditions (150°C–200°C)," in *Proc. 6th Int. Conf. Integr. Power Electron. Syst.*, 2010, pp. 1–3.
[66] M. A. Huque, S. K. Islam, L. M. Tolbert, and B. J. Blalock, "A 200 °C universal gate driver integrated circuit for extreme environment applications," *IEEE Trans. Power Electron.*, vol. 27, no. 9, pp. 4153–4162, Sep. 2012.
[67] J. Valle-Mayorga *et al.*, "High-temperature silicon-on-insulator gate driver for SiC-FET power modules," *IEEE Trans. Power Electron.*, vol. 27, no. 11, pp. 4417–4424, Nov. 2012.
[68] CISSOID, "High temperature half-bridge driver," CHT-HYPERION Datasheet, Feb. 2021 [*Revision: 1.8*].
[69] R. R. Lamichhane *et al.*, "A wide bandgap silicon carbide (SiC) gate driver for high-temperature and high-voltage applications," in *Proc. 26th Int. Symp. Power Semicond. Devices ICs*, 2014, pp. 414–417, doi: 10.1109/ISPSD.2014.6856064.
[70] S. Kargarrazi, H. Elahipanah, Z. Tong, D. Senesky, and C. Zetterling, "500°C SiC-based driver IC for SiC power MOSFETs," in *Proc. 31st Int. Symp. Power Semicond. Devices ICs*, 2019, pp. 115–118, doi: 10.1109/ISPSD.2019.8757618.
[71] M. Barlow, S. Ahmed, A. M. Francis, and H. A. Mantooth, "An integrated SiC CMOS gate driver for power module integration," *IEEE Trans. Power Electron.*, vol. 34, no. 11, pp. 11191–11198, Nov. 2019.
[72] F. Qi, L. Xu, J. Ping, G. Zhao, and J. Wang, "High temperature gate drive circuit for SiC power MOSFET application," in *Proc. IEEE Conf. Expo Transp. Electrific. Asia-Pacific*, 2014, pp. 1–6, doi: 10.1109/ITEC-AP.2014.6941030.
[73] F. Qi and L. Xu, "Development of a high-temperature gate drive and protection circuit using discrete components," *IEEE Trans. Power Electron.*, vol. 32, no. 4, pp. 2957–2963, Apr. 2017.
[74] P. Nayak, S. K. Pramanick, and K. Rajashekara, "A high-temperature gate driver for silicon carbide mosfet," *IEEE Trans. Ind. Electron.*, vol. 65, no. 3, pp. 1955–1964, Mar. 2018.
[75] Texas Instruments, "Comparing shunt- and hall-based isolated current-sensing solutions in HEV/EV," SBAA 293B, Jun. 2018 [*Revised:* Jan. 2019].
[76] P. Ning, F. Wang, and K. D. T. Ngo, "250°C SiC high density power module development," in *Proc. 26th Annu. IEEE Appl. Power Electron. Conf. Expo.*, 2011, pp. 1275–1281, doi: 10.1109/APEC.2011.5744757.
[77] ALLEGRO microsystems, "400 kHz, high accuracy current sensor," ACS37002 Datasheet, 2021 [*ACS37002-DS, Rev. 7*].
[78] B. Wrzecionko, L. Steinmann, and J. W. Kolar, "High-bandwidth high-temperature (250 °C/500 °F) isolated DC and AC current measurement: Bidirectionally saturated current transformer," *IEEE Trans. Power Electron.*, vol. 28, no. 11, pp. 5404–5413, Nov. 2013.
[79] J. Watson and P. Maithil, "Harsh environment conquered - low power, precision, high temperature components for extreme high temperature applications," *Analog Devices MS-2707*, 2014. [Online]. Available: https://www.analog.com/media/en/technical-documentation/tech-articles/harsh-environments-conquered-low%20power-precision-high-temperature-components-for-extreme-high-temperature-applications-ms-2707.pdf
[80] CISSOID, "High temperature & extended lifetime semiconductors," *Product Catalog*.
[81] XREL semiconductor, "High-temperature low-power series voltage regulator XTR75010," DS-00034-11, 2019-02-05 [Rev. 5H].
[82] IISB Fraunhofer, "4H-SiC high temperature sensing & electronics," *Product Sheet*.
[83] XREL semicond., "High-temperature isolated two-channel transceiver," DS-00400-13, 2021 [Rev. 3].
[84] Texas Instrum., "SM320F28335-HT digital signal controller (DSC)" Data Manual, Dec. 2010 [Rev. Jan. 2014].
[85] Texas Instrum., "SM320F2812-HT digital signal processor," Data Manual, Jun. 2009 [*Rev*. Jun. 2011].
[86] D. Shaddock and L. Yin, "*Reliability of high temperature laminates*," Additional Conferences (Device Packaging, HiTEC, HiTEN, and CICMT)Jul. 2015; 2015 (HiTEN): 000 100–000110. doi: 10.4071/HiTEN-Session3b-Paper3b_1.
[87] O.Aviño Salvado, W.C. SabbahHervé ButtayP. MorelBevilacqua, "Evaluation of printed-circuit boards materials for high temperature operation," HiTEN, IMAPS, Jul. 2017, Cambridge, UK.

[88] F. Bechtold, “A comprehensive overview on today’s ceramic substrate technologies,” in *Proc. Eur. Microelectron. Packag. Conf.*, 2009, pp. 1–12.
[89] IPC-A-610 Acceptability of Electronics Assemblies Endorsement Program.
[90] R. Wang *et al.*, “A high-temperature SiC three-phase AC–DC converter design for $>$ 100 °C ambient temperature,” *IEEE Trans. Power Electron.*, vol. 28, no. 1, pp. 555–572, Jan. 2013.
[91] F. Qi, M. Wang, L. Xu, B. Zhao, Z. Zhou, and X. Ren, “Design and evaluation of 30 kVA inverter using SiC MOSFET for 180°C ambient temperature operation,” in *Proc. IEEE Appl. Power Electron. Conf. Expo.*, 2016, pp. 2912–2918, doi: 10.1109/APEC.2016.7468277.
[92] F. Qi, M. Wang, and L. Xu, “Investigation and review of challenges in a high-temperature 30-kVA three-phase inverter using SiC mosfets,” *IEEE Trans. Ind. Appl.*, vol. 54, no. 3, pp. 2483–2491, May/Jun. 2018.
[93] R. M. Nelms and R. W. Johnson, “200 °C operation of a 500-W DC–DC converter utilizing power mosfets,” *IEEE Trans. Ind. Appl.*, vol. 33, no. 5, pp. 1267–1272, Sep./Oct. 1997.
[94] B. Ray and R. L. Spyker, “High temperature design and testing of a DC–DC power converter with Si and SiC devices,” in *Proc. Conf. Rec. IEEE Ind. Appl. Conf., 39th IAS Annu. Meeting*., 2004, vol. 2, pp. 1261–1266, doi: 10.1109/IAS.2004.1348574.
[95] B. Ray, J. D. Scofield, R. L. Spyker, B. Jordan, and S.-H. Ryu, “High temperature operation of a DC–DC power converter utilizing SiC power devices,” in *Proc. 20th Annu. IEEE Appl. Power Electron. Conf. Expo.*, 2005, pp. 315–321, doi: 10.1109/APEC.2005.1452944.
[96] S. Krishnaswami *et al.*, “1000-V, 30-A 4H-SiC BJTs with high current gain,” *IEEE Electron Device Lett.*, vol. 26, no. 3, pp. 175–177, Mar. 2005, doi: 10.1109/LED.2004.842731.
[97] B. Ray, H. Kosai, J. D. Scofield, and B. Jordan, “200 °C operation of a DC–DC converter with SiC power devices,” in *Proc. APEC - 22nd Annu. IEEE Appl. Power Electron. Conf. Expo.*, 2007, pp. 998–1002, doi: 10.1109/APEX.2007.357636.
[98] R. Spyker, J. Huth, I. Mehdi, and A. Brockschmidt, “300 °C ferrite material for high temperature magnetics,” in *Proc. IEEE 35th Annu. Power Electron. Specialists Conf.*, 2004, pp. 155–160, doi: 10.1109/PESC.2004.1355733.
[99] H. Kosai, J. Scofield, S. McNeal, B. Jordan, and B. Ray, “Design and performance evaluation of a 200 °C interleaved boost converter,” *IEEE Trans. Power Electron.*, vol. 28, no. 4, pp. 1691–1699, Apr. 2013.
[100] M. S. Duraij, Y. Xiao, G. Zsurzsan, and Z. Zang, “Enhancement mode GaN-FETs in extreme temperature conditions–Part I: Static parasitic parameters, additional conferences (device packaging, HiTEC, HiTEN, and CICMT),” Apr. 2021; 2021 (HiTEC): 0000 48–000052. doi: 10.4071/2380-4491.2021.HiTEC.000048.
[101] Martijn S. Duraij, Y. Xiao, G. Zsurzsan, and Z. Zang, “Enhancement mode GaN-FETs in extreme temperature conditions–Part II: Dynamic parasitic parameters. additional conferences (device packaging, HiTEC, HiTEN, and CICMT),” Apr. 2021; 2021 (HiTEC): 0000 53–000057. doi: 10.4071/2380-4491.2021.HiTEC.000053.
[102] Y. Xiao, M. Duraij, Z. Zhang, G. Zsurzsan, M. Hansen, and B. Thomsen, “Design automation combining analytical models and numerical simulations for three-level neutral-point-clamped DC-DC converter,” in *Proc. IEEE Des. Methodologies Conf.*, 2021, pp. 1–6, doi: 10.1109/DMC51747.2021.9529930.
[103] Magnetics Inc., “Effects of temperature on core loss of alloy powder cores.” [Online]. Available: https://www.mag-inc.com/Media/Magnetics/File-Library/Product%20Literature/Powder%20Core%20Literature/Effects-of-Temperature-on-Core-Loss-of-Alloy-Powder-Cores.pdf

**Yudi Xiao** received the B.Sc. and M.Sc. degrees in power electronics from Fuzhou University, Fuzhou, China, in 2015 and 2018, respectively. He is currently working toward the Ph.D. degree with the Department of Electrical Engineering, Technical University of Denmark, Kongens Lyngby, Denmark.

**Zhe Zhang** (Senior Member, IEEE) received the B.Sc. and M.Sc. degrees in power electronics from Yanshan University, Qinhuangdao, China, in 2002 and 2005, respectively, and the Ph.D. degree from the Technical University of Denmark, Kongens Lyngby, Denmark, in 2010.

From 2014 to 2021, he was an Associate Professor with the Department of Electrical Engineering, Technical University of Denmark (DTU), where he has been the Head of Studies in charge of Electrical Engineering M.Sc. Programme since January 2018. From 2005 to 2007, he was an Assistant Professor with Yanshan University. From June 2010 to August 2010, he was a Visiting Scholar with the University of California, Irvine, CA, USA. He was an Assistant Professor with the Technical University of Denmark during 2011 and 2014. He has authored or co-authored more than 200 transactions and international conference papers and filed over 10 patent applications. His research interests include applications of wide bandgap devices, high-frequency dc–dc converters, dc–ac inverters, high-frequency magnetics for renewable energy systems, hybrid electric vehicles, high-temperature power solutions, and piezoelectric-actuator, piezoelectric-transformer-based power converters.

Dr. Zhang was the recipient of the awards and honors, including Best Paper Awards in IEEE conferences of ECCE, IFEEC, and IGBSG, Best Teacher of the Semester, Chinese Government Award for Outstanding Students Abroad, etc. He is an Associate Editor for the IEEE TRANSACTIONS ON INDUSTRIAL ELECTRONICS, *IEEE Journal of Emerging and Selected Topics in Power Electronics*, and *IEEE Access*, and Guest Editor for the *IEEE Journal of Emerging and Selected Topics in Industrial Electronics*.

**Martijn Sebastiaan Duraij** received the B.Sc. degree, in 2013, from the Fontys University of Applied Sciences, Eindhoven, The Netherlands, and the M.Sc. degree, in 2015, from the Technical University of Denmark, Kongens Lynby, Denmark, where he is currently working toward the Ph.D. degree with the Department of Electrical Engineering.

He has worked in the industries for several years.

**Tiberiu-Gabriel Zsurzsan** received the B.Sc. degree in applied electronics from the Polytechnic University of Timisoara, Timisoara, Romania, in 2010, and the M.Sc. degree in automation and robotics and the Ph.D. degree from the Technical University of Denmark, Kongens Lyngby, Denmark, in 2012 and 2016, respectively.

He is currently an Associate Professor with the Technical University of Denmark. His research interests include sensing and sensor systems, human motion tracking, harsh environment electronics, modeling and control of exotic motors, as well as piezoelectric vibrations.

**Michael A. E. Andersen** (Member, IEEE) received the M.Sc.E.E. and Ph.D. degrees in power electronics from the Technical University of Denmark, Kongens Lyngby, Denmark, in 1987 and 1990, respectively.

He is currently a Professor of power electronics with the Technical University of Denmark, where he has been the Deputy Head of the Department of Electrical Engineering since 2009. He is the author or coauthor of more than 300 publications. His research interests include switch-mode power supplies, piezoelectric transformers, power factor correction, and switch-mode audio power amplifiers.